SUPPORTING INFORMATION

Titanocene Pnictinidene Complexes

Dr. Malte Fischer, Dr.Fabian Reiß, Dr. Christian Hering-Junghans

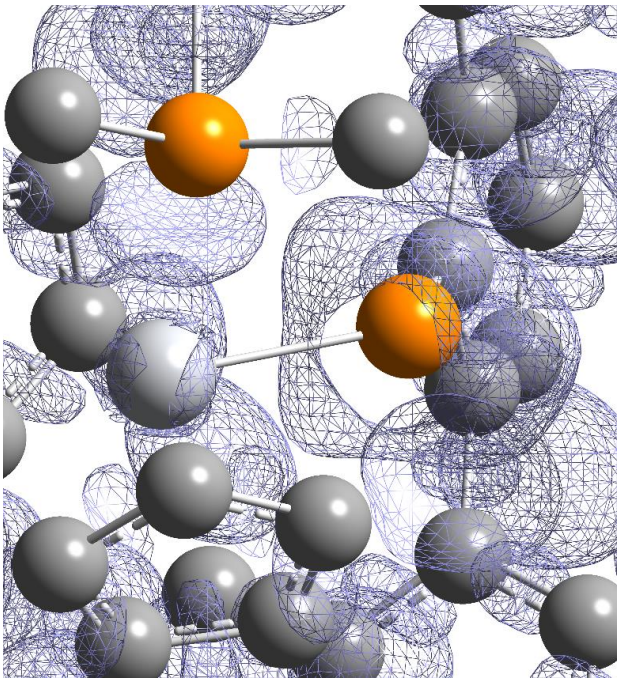

This file includes:

1 Experimental

General Information. If not stated otherwise, all manipulations were performed under oxygen- and moisture-free conditions under an inert atmosphere of argon using standard Schlenk techniques or an inert atmosphere glovebox (MBraun LABstar ECO). All glassware was heated three times *in vacuo* using a heat gun and cooled under argon atmosphere. Solvents were transferred using syringes, steel- or PE-canulas, which were purged with argon prior to use. Solvents and reactants were either obtained from commercial sources or synthesized as detailed in Table S1.

Table S1: Origin and purification of solvents and reactants.

Substance	Origin	Purification
Benzene	local trade	dried over Na/benzophenone freshly distilled prior to use, stored over molecular sieves.
n-pentane	local trade	dried over Na/benzophenone/tetraglyme freshly distilled prior to use
THF	Sigma Aldrich, inhibitor-free, for HPLC, ≥99.9%	purified with the Grubbs-type column system "Pure Solv MD-5" dried over Na/benzophenone freshly distilled prior to use
C_6D_6	euriso-top	dried over Na/benzophenone freshly distilled prior to use
C_7D_8 (toluene-d_8)	euriso-top	dried over Na/benzophenone freshly distilled prior to use
$Cp_2Ti(C_2(SiMe_3)_2)$[1]	synthesized	
$^{Dip}TerPPMe_3$[2]	synthesized	
$^{Dip}TerAsPMe_3$[3]	synthesized	
$^{Mes}TerPPMe_3$[2]	synthesized	
Mes*$PPMe_3$[2]	synthesized	

NMR spectra were recorded on Bruker spectrometers (AVANCE 300, AVANCE 400 or Fourier 300) and were referenced internally to the deuterated solvent (^{13}C: C_6D_6 δ_{ref} = 128.06 ppm; C_7D_8 δ_{ref} = 20.43 ppm) or to protic impurities in the deuterated solvent (^{1}H: C_6HD_5 δ_{ref} = 7.16 ppm; C_7D_8 δ_{ref} = 2.08 ppm). All measurements were carried out at ambient temperature unless denoted otherwise. NMR signals were assigned using experimental data (e.g. chemical shifts, coupling constants, integrals where applicable).

Elemental analyses were obtained using a Leco Tru Spec elemental analyzer.

Mass spectra were recorded on a Thermo Electron MAT 95-XP sector field mass spectrometer using crystalline samples.

UV-Vis analysis was performed using an *analytikjena specord s* 600 diode array photometer. The samples were dissolved in THF in a drybox in a 1 cm quartz cuvette with a Schlenk-Valve. If necessary, the samples were diluted using Schlenk techniques.

2 Structure elucidation

X-ray Structure Determination: X-ray quality crystals of **3** and **5** were selected in Fomblin© Y perfluoroether (Sigma Aldrich) at −30 °C under a constant stream of nitrogen. X-ray quality crystals of **6_i** and **6_ii** were selected in Fomblin© Y-1800 perfluoroether (Alfa Aesar) at room temperature. The samples were cooled to 150(2) K during measurement. The data were collected on a Bruker Kappa Apex II diffractometer using Mo K_α radiation (λ = 0.71073 Å) or Cu K_α radiation (λ = 1.54178 Å). The structures were solved by iterative methods (SHELXT)[4] and refined by full matrix least squares procedures (SHELXL).[5] Semi-empirical absorption corrections were applied (SADABS).[6] All non-hydrogen atoms were refined anisotropically, hydrogen atoms were included in the refinement at calculated positions using a riding model.

The structure of **3** was refined as a two-component twin.

In the asymmetric unit of **5** eight severely disordered n-hexane molecules were found. These solvent molecules have been treated as a diffuse contribution to the overall scattering by using PLATON/SQUEEZE.[7]

For **6** two modifications could be obtained. In **6_ii** the central As2 unit was found to be disordered and was split in two parts. The occupancy of each part was allowed to refine freely.

Table S2: Crystallographic details of **3**, **5** and **6_i**.

Compound	**3**	**5**	**6_i**
Chem. Formula	$C_{37}H_{44}P_2Ti$	$C_{43}H_{56}PAsTi$ 1.33 (C_6H_{14})	$C_{60}H_{74}As_2$
Formula weight [g/mol]	598.56	841.56	945.03
Colour	black	brown	yellow
Crystal system	monoclinic	triclinic	monoclinic
Space group	$P2_1/c$	P-1	$C2/c$
a [Å]	16.6969(8)	17.7808(5)	21.4486(15)
b [Å]	10.4621(5)	19.3646(5)	14.9005(10)
c [Å]	18.3000(8)	21.7658(5)	16.0230(11)
α [°]	90	79.424(2)	90
β [°]	99.112(2)	81.436(2)	95.2270(13)
γ [°]	90	89.781(2)	90
V [Å^3]	3156.4(3))	7282.8(3)	5099.6(6)
Z	4	6	4
$\rho_{calcd.}$ [g/cm^3]	1.260	1.151	1.231
μ [mm^{-1}]	3.424	2.716	1.347
T [K]	150(2)	150(2)	150(2)
Measured reflections	26770	103642	38522
Independent reflections	5650	24760	7447
Reflections with $I > 2\sigma(I)$	5490	18627	5712
R_{int}	0.0375	0.0609	0.0334
$F(000)$	1272	2704	2000
$R_1(R[F^2>2\sigma(F^2)])$	0.0311	0.0505	0.0315
$wR_2(F^2)$	0.0870	0.1423	0.0836
GooF	1.057	1.025	1.024
No. of Parameters	371	1317	288
CCDC #	2060154	2060155	2060156

Table S3: Crystallographic details of **6_ii**.

Compound	**6_ii**
Chem. Formula	$C_{60}H_{74}As_2 \cdot 2(C_6H_6)$
Formula weight [g/mol]	1101.24
Colour	orange
Crystal system	Triclinic
Space group	*P*-1
a [Å]	13.2848(10)
b [Å]	14.6046(12)
c [Å]	16..1967(13)
α [°]	97.9377(29)
β [°]	97.4838(28)
γ [°]	96.5107(29)
V [Å^3]	3058.1(4)
Z	2
$\rho_{calcd.}$ [g/cm^3]	1.196
μ [mm^{-1}]	1.133
T [K]	150(2)
Measured reflections	102903
Independent reflections	16266
Reflections with $I > 2\sigma(I)$	14004
R_{int}	0.0301
F(000)	1168
$R_1(R[F^2>2\sigma(F^2)])$	0.0297
$wR_2(F^2)$	0.0800
GooF	1.036
No. of Parameters	739
CCDC #	2060157

Figure S1: Molecular structure of **3**. ORTEPs drawn at 50% probability, all H-atoms omitted and Mes-groups rendered as wireframe for clarity. Selected bond lengths (Å) and angles (°) of **3**: C1–P1 1.8417(18), Ti1–P1 2.4225(6), Ti1–P2 2.5688(6), Ti1–Ct1 2.0491(3), Ti1–Ct2 2.0770(3); C1–P1–Ti1 122.12(6), P1–Ti1–P2 86.823(19), Ct1–Ti1–Ct2 135.374(18), Ct2–Ti1–P1 111.213(17), Ct1–Ti1–P2 105.424(19), Ct2–Ti1–P1 104.007(17), Ct2–Ti1–P2 102.986(18); C6–C1–P1–Ti1 –2.05(18).

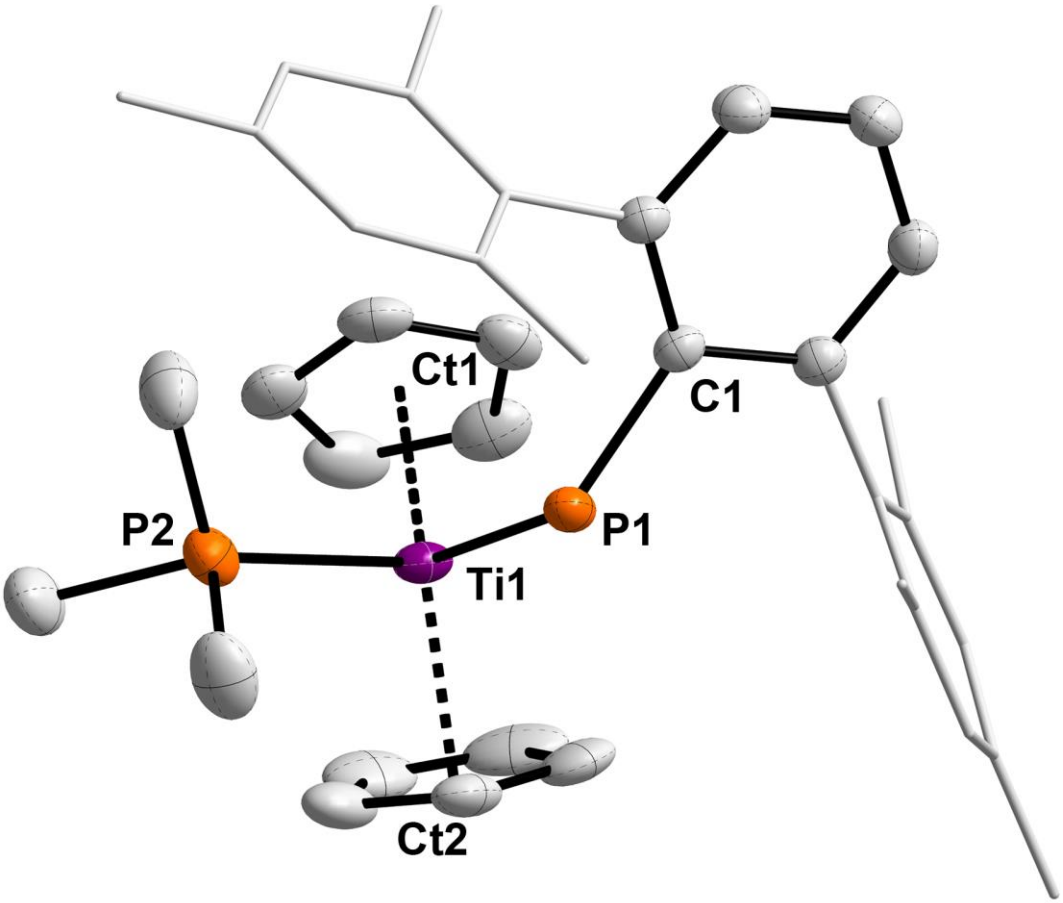

Figure S2: Molecular structure of **5** showing all three independent molecules in the asymmetric unit. ORTEPs drawn at 30% probability, all H-atoms omitted and Dip-groups rendered as wireframe for clarity. Selected bond lengths (Å) and angles (°) of **5**: (*1*) C1–As1 1.989(3), Ti1–As1 2.4726(8), Ti1–P1 2.5545(11), Ti1–Ct1 2.0585(6), Ti1–Ct2 2.0292(7); C1–As1–Ti1 121.73(10), P1–Ti1–As1 88.05(3), Ct1–Ti1–Ct2 136.128(35), Ct2–Ti1–As1 109.337(30), Ct1–Ti1–P1 104.260(34), Ct2–Ti1–As1 103.156(26), Ct2–Ti1–P1 105.498(34); Ti1–As1–C1–C2 –97.723(246); (*2*) C44–As2 1.985(3), Ti2–As2 2.4638(9), Ti2–P2A 2.549(3), Ti2–Ct3 2.0702(6), Ti2–Ct4 2.0300(7); C44–As2–Ti2 121.63(9), As2–Ti2–P2A 92.49(18), Ct3–Ti2–Ct4 136.251(37), Ct4–Ti2–P2A 101.949(104), Ct3–Ti2–As2 102.878(27), Ct3–Ti2–P2A 105.817(89), Ct4–Ti2–As2 109.015(34); Ti2–As2–C43–C44 –99.118(280); (*3*) C87–As3 2.008(4), Ti3–As3 2.4659(9), Ti3–P3 2.5526(13), Ti3–Ct5 2.0698(6), Ti3–Ct6 2.0218(6); C87–As3–Ti3 123.22(11), P3–Ti3–As3 89.31(4), Ct5–Ti3–Ct6 135.590(33), Ct6–Ti3–As3 108.447(29), Ct5–Ti3–P1 104.525(38), Ct5–Ti3–As3 103.880(31), Ct6–Ti3–P3 105.475(38); Ti3–As3–C87–C88 –94.946(277).

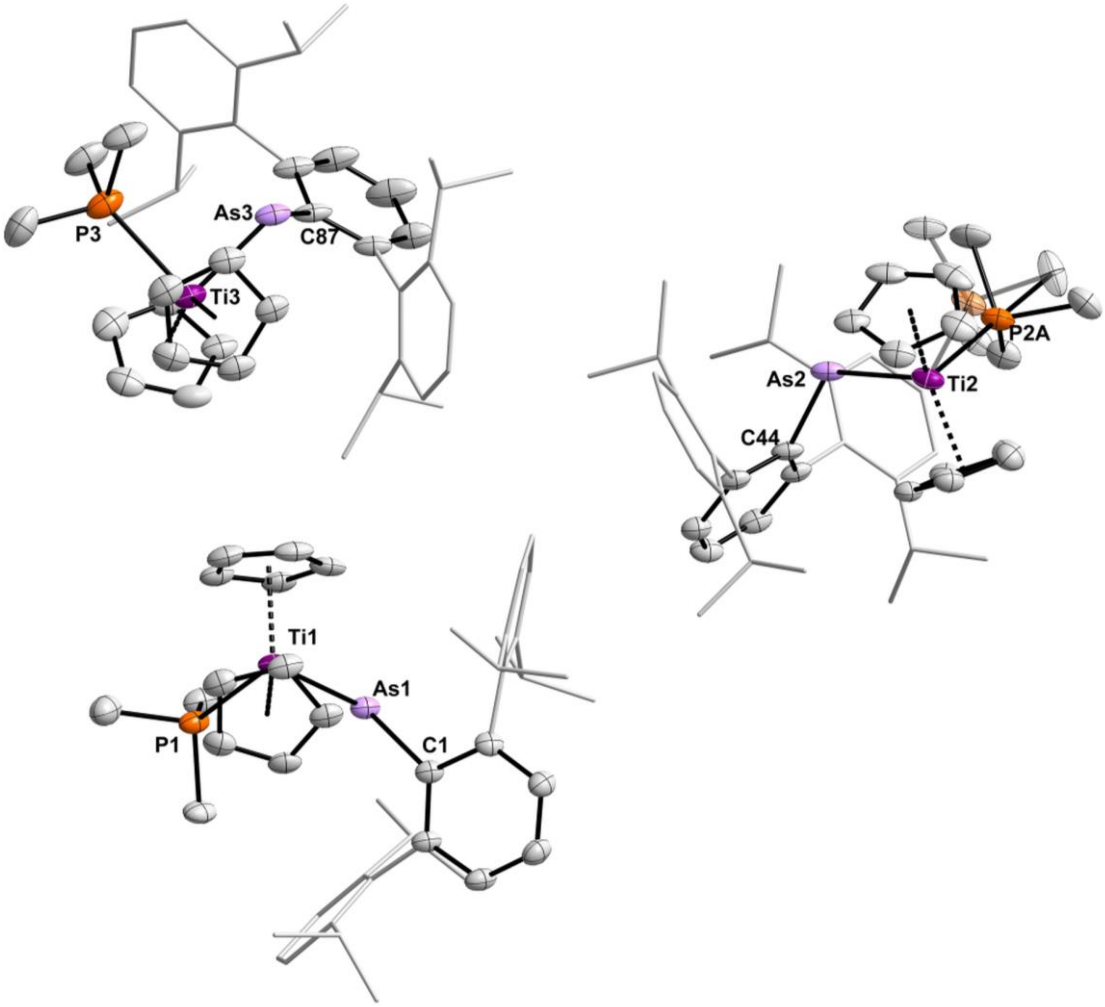

Figure S3: Molecular structure of **6_i**. ORTEPs drawn at 50% probability, all H-atoms omitted and Dip-groups rendered as wireframe for clarity. The molecule lies on an inversion center. Labels with added prime indicate symmetry equivalent positions (3/2-x, 3/2-y, 1-z). Selected bond lengths (Å) and angles (°) of **6_i**: C1−As1 1.9901(13), As1−As1′ 2.2679(3); C1−As1−As1′ 101.15(4); C2−C1−As1−As1′ −95.725(109).

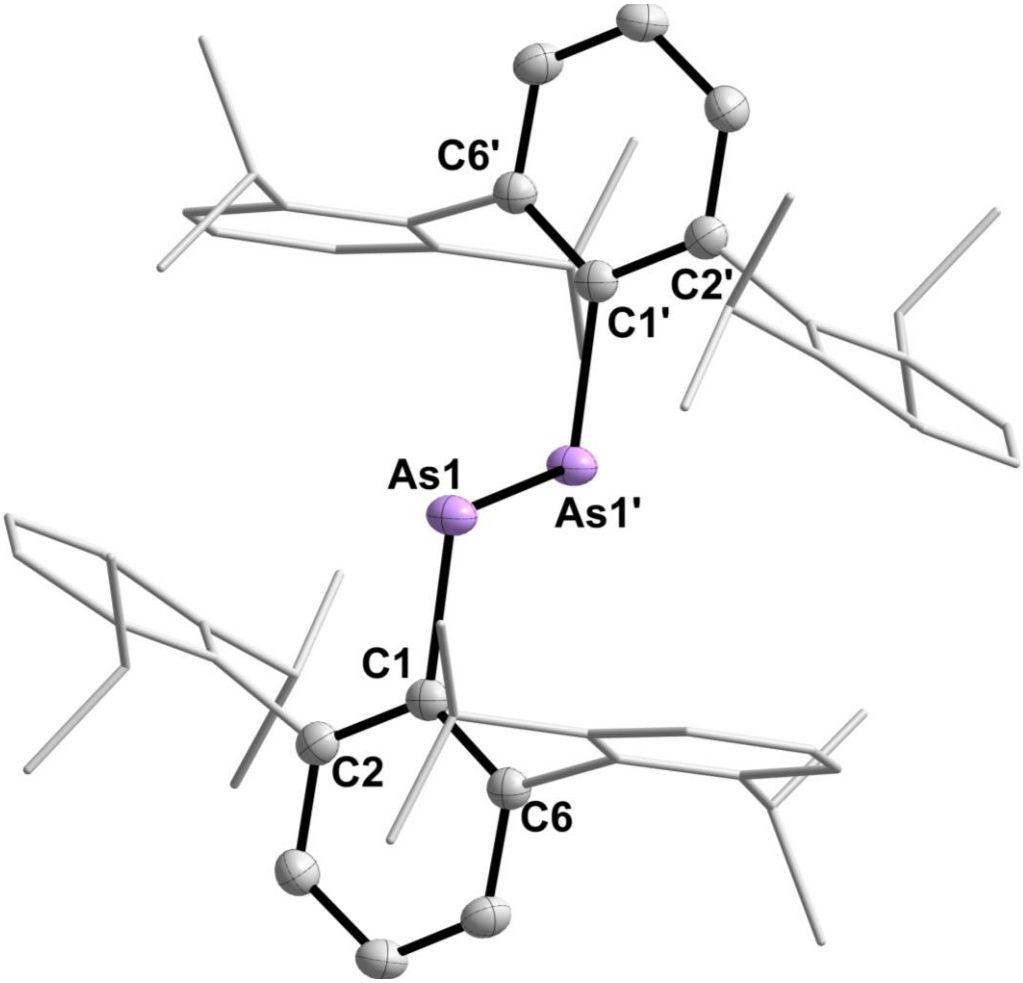

Figure S4: Molecular structure of **6_ii**. ORTEPs drawn at 50% probability, all H-atoms and two benzene molecules associated with **6_ii** omitted and Mes-groups rendered as wireframe for clarity. The occupancy of the major orientation is 0.9438(13), whereas the minor orientation is 0.0562(13). Selected bond lengths (Å) and angles (°) of **3**: C1−As1A 1.9929(12), C31−As2A 1.9764(12), As1A−As2A 2.2659(3), As1B−As2B 2.355(6); C1−As1A−As2A 96.61(3), C31−As2A−As1A 108.62(4); C6−C1−As1A−As2A 78.869(98), C32−C31−As2A−As1A −16.112(116).

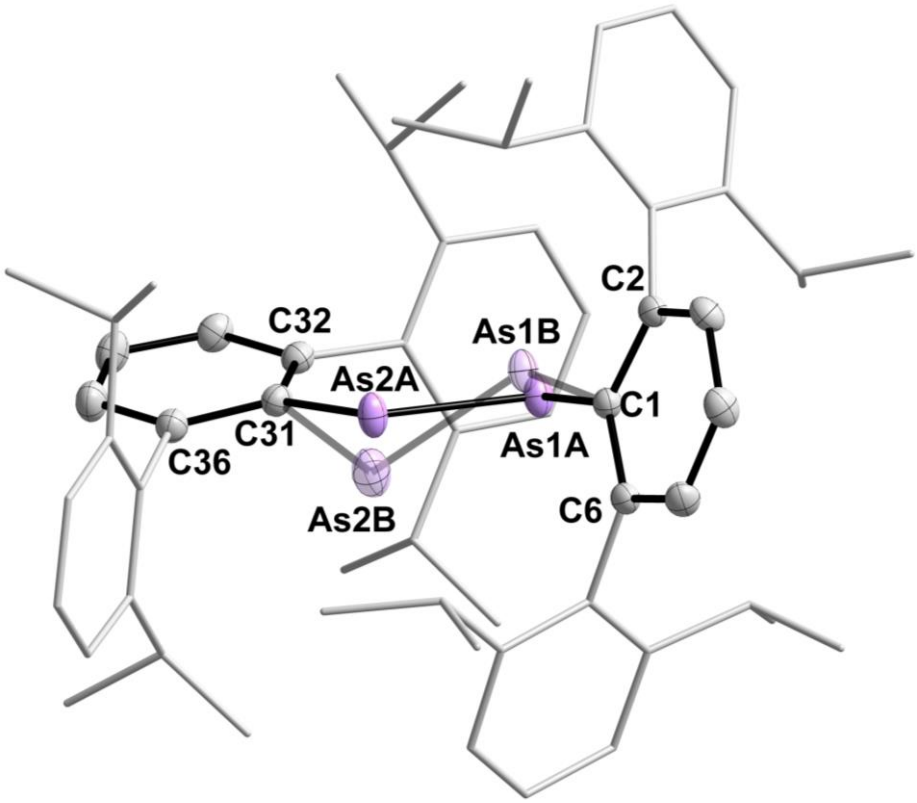

3 Attempted Syntheses of $Cp_2Ti(PMe_3)PR$ (R = Mes*, ^{Dip}Ter)

3.1 Attempted Synthesis of $Cp_2Ti(PMe_3)PMes^*$

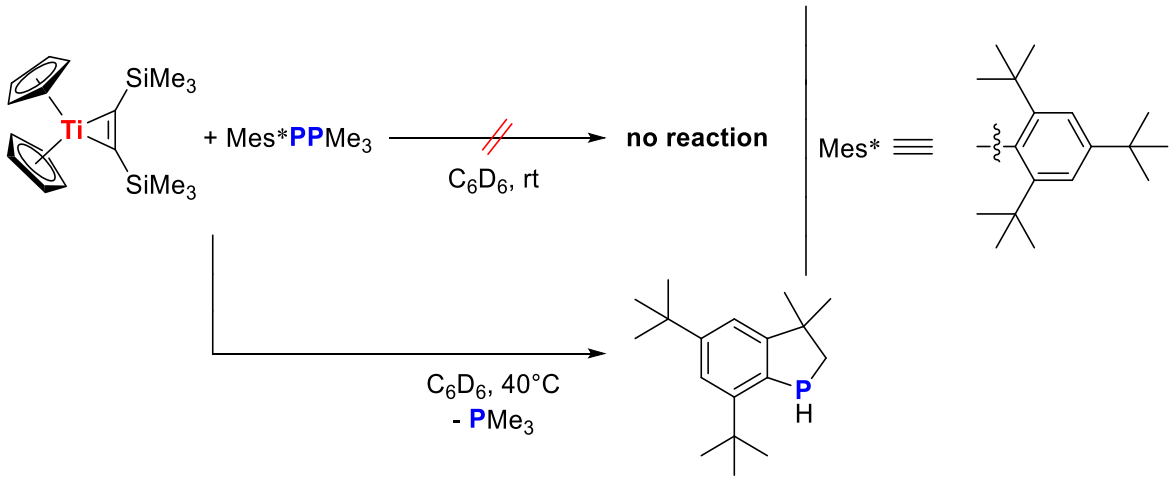

In a Young NMR tube $Cp_2Ti(btmsa)$ (**1**) (0.022 g, 0.063 mmol) and Mes^*PPMe_3 (**2a**) (0.022 g, 0.063 mmol) were dissolved in 0.6 mL of C_6D_6. The reaction mixture was allowed to stand for 16 h at room temperature. Regular control by ^1H and $^{31}P\{^1H\}$ NMR spectroscopy showed that no reaction has occurred. Subsequent heating of the reaction mixture to 40 °C for two hours results mainly in the formation of 3,3-dimethyl-5,7-di-*tert*-butylphosphaindane (**A**) (Figures S5-S7).

^{1}H NMR (300 MHz, C_6D_6, 298 K): δ = 1.12 (s, 3H, $C_q(CH_3)_2$), 1.30-1.32 (m, 12H, $C_q(CH_3)_2$, $C_q(CH_3)_3$), 1.57 (s, 9H, $C_q(CH_3)_3$), 1.69-1.75 (m, 2H, $PHCH_2$), 4.40 (dm, $^1J_{P,H}$ = 181.6 Hz, PH), 7.16 (m, 1H, CH_{Aryl})*, 7.46-7.48 (m, 1H, CH_{Aryl}) ppm.

* = overlap with C_6D_5H signal

$^{13}C\{^1H\}$ NMR (75 MHz, C_6D_6, 298 K): δ = 27.5 ($C_q(\underline{C}H_3)_2$), 30.3 ($C_q(\underline{C}H_3)_2$), 31.3 (d, $J_{P,C}$ = 10.0 Hz, $C_q(\underline{C}H_3)_3$), 31.7 ($C_q(\underline{C}H_3)_3$), 35.1 ($\underline{C}_q(CH_3)_3$), 35.6 (d, $^1J_{P,C}$ = 4.9 Hz, PCH_2), 31.7 ($\underline{C}_q(CH_3)_3$), 47.0 (d, $^2J_{P,C}$ = Hz, $\underline{C}_q(CH_3)_2$), 117.9 (d, $^3J_{P,C}$ = 1.2 Hz, CH_{Aryl}), 121.4 (d, $^3J_{P,C}$ = 4.9 Hz, CH_{Aryl}), 130.0 (d, $^2J_{P,C}$ = 14.9 Hz, $C_{q,Aryl}$), 151.7 ($C_{q,Aryl}$), 152.9 (d, $^1J_{P,C}$ = 14.2 Hz, $C_{q,Aryl}$), 157.4 ($C_{q,Aryl}$) ppm.

$^{31}P\{^1H\}/^{31}P$ NMR (122 MHz, C_6D_6, 298 K): δ = -79.7 (dm, $^1J_{P,H}$ = 181.9 Hz) ppm.

Figure S5: ^{1}H NMR spectrum of the reaction of $Cp_2Ti(btmsa)$ (**1**) with Mes*$PPMe_3$ (**2a**) (300 MHz, C_6D_6, rt); -0.25 and 6.26 ppm: $Cp_2Ti(btmsa)$, 0.15 ppm: btmsa.

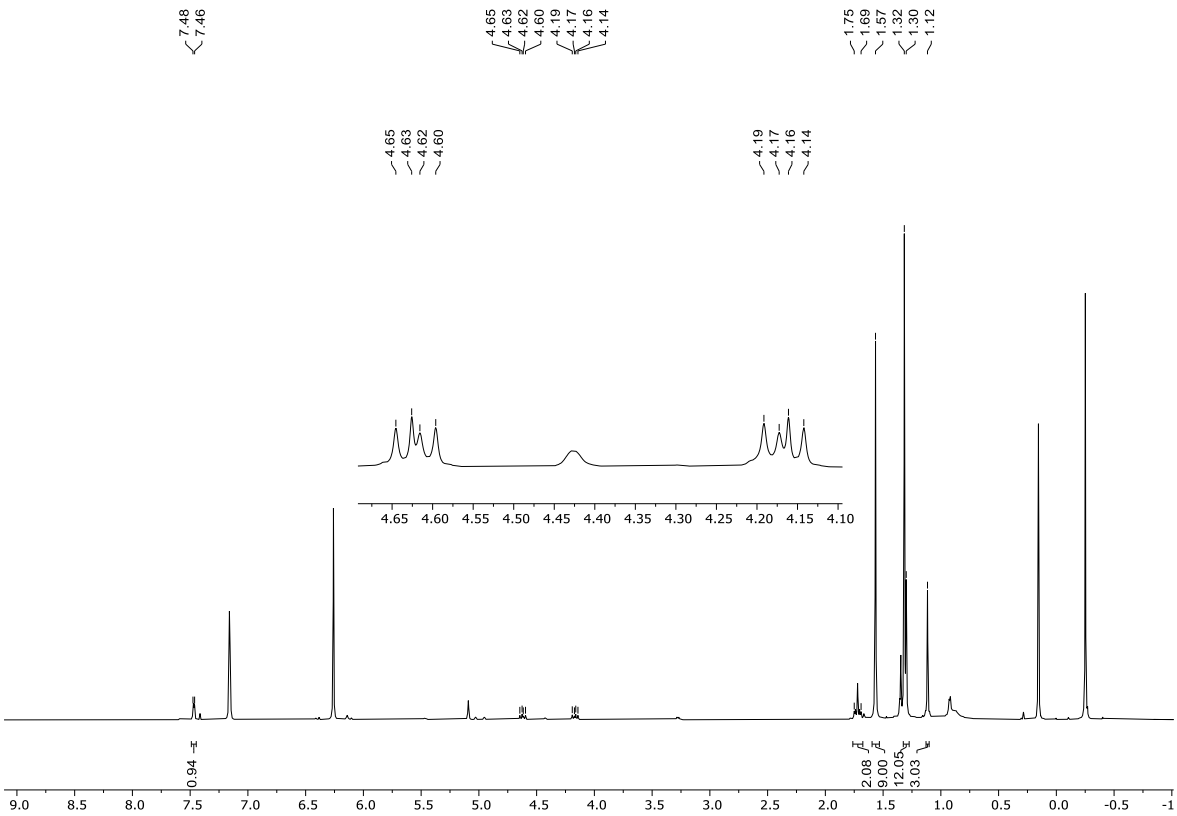

Figure S6: $^{13}C\{^{1}H\}$ NMR spectrum of the reaction of $Cp_2Ti(btmsa)$ (**1**) with Mes*$PPMe_3$ (**2a**) (75 MHz, C_6D_6, rt); 0.9 and 116.2 ppm: $Cp_2Ti(btmsa)$, 0.0 ppm: btmsa.

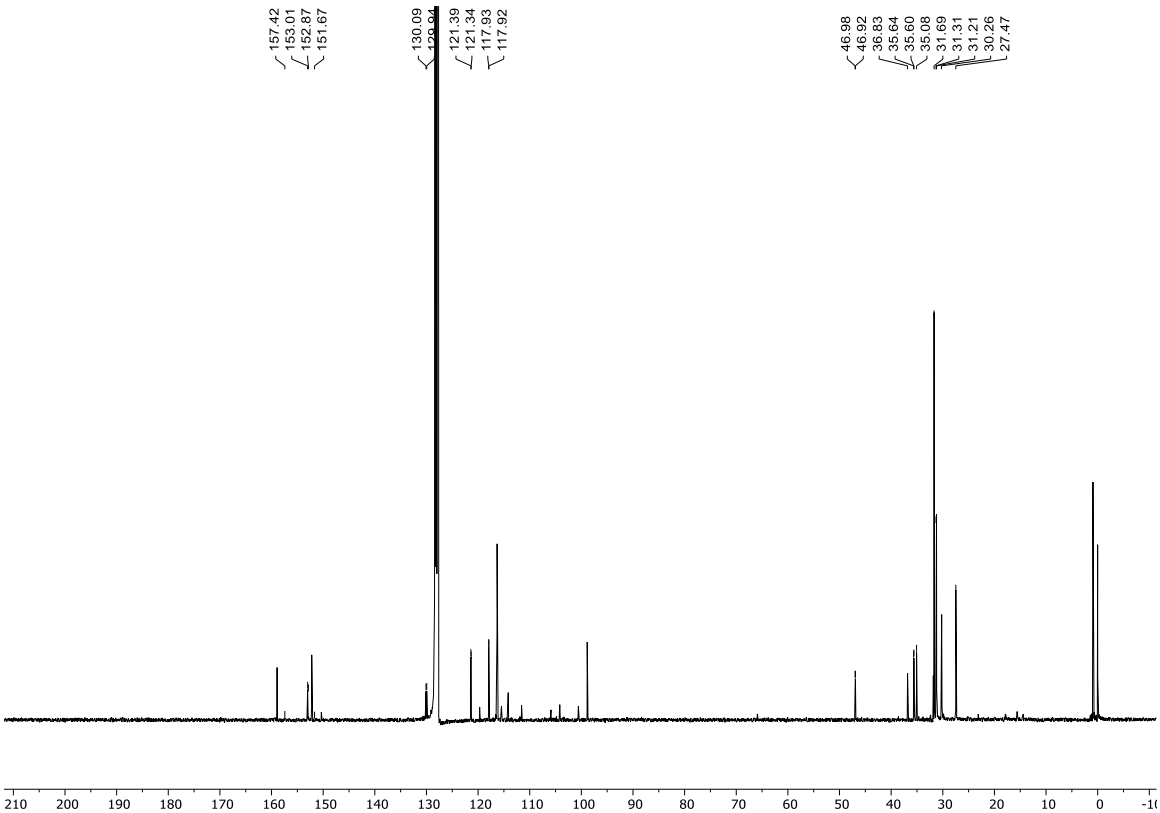

Figure S7: $^{31}P\{^{1}H\}$ (bottom) and ^{31}P NMR (top) spectra of the reaction of $Cp_2Ti(btmsa)$ (**1**) with Mes^*PPMe_3 (**2a**) (122 MHz, C_6D_6, rt).

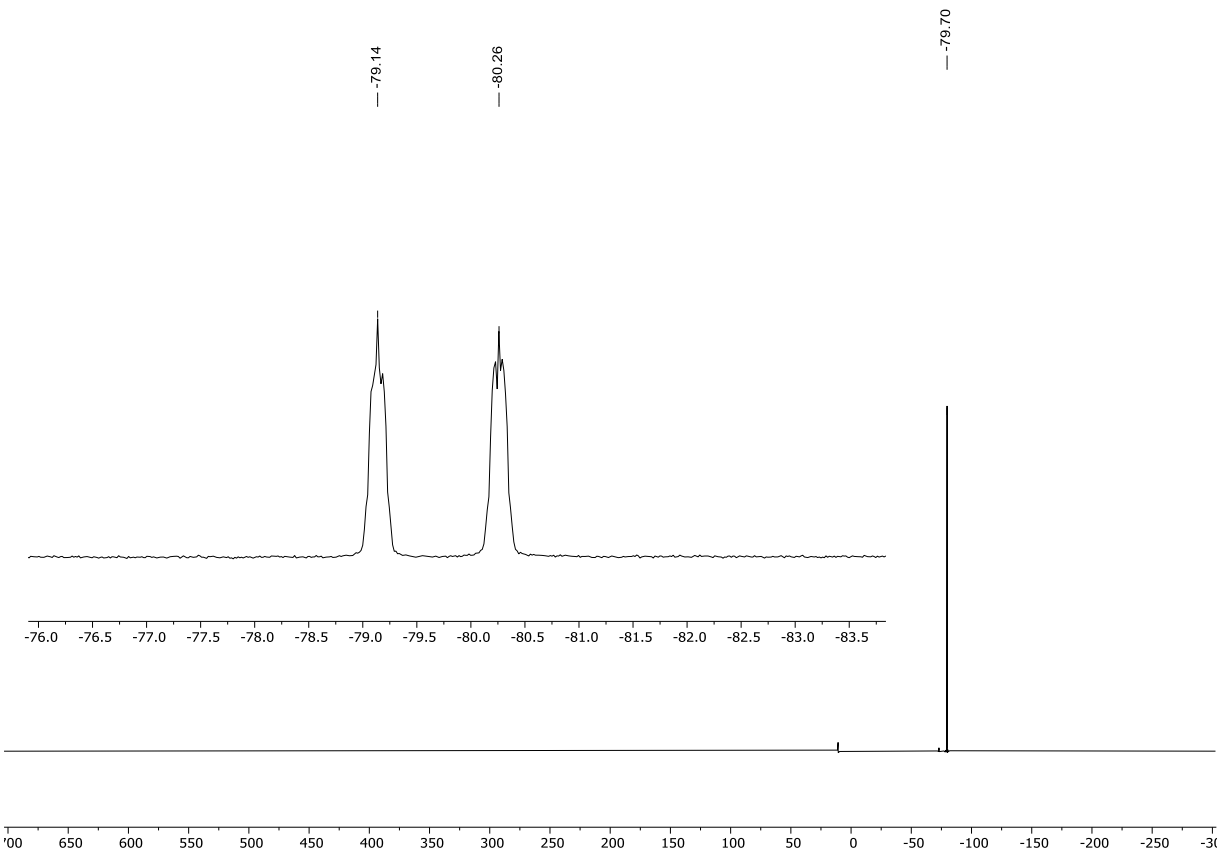

3.2 Attempted Synthesis of $Cp_2Ti(PMe_3)P^{Dip}Ter$

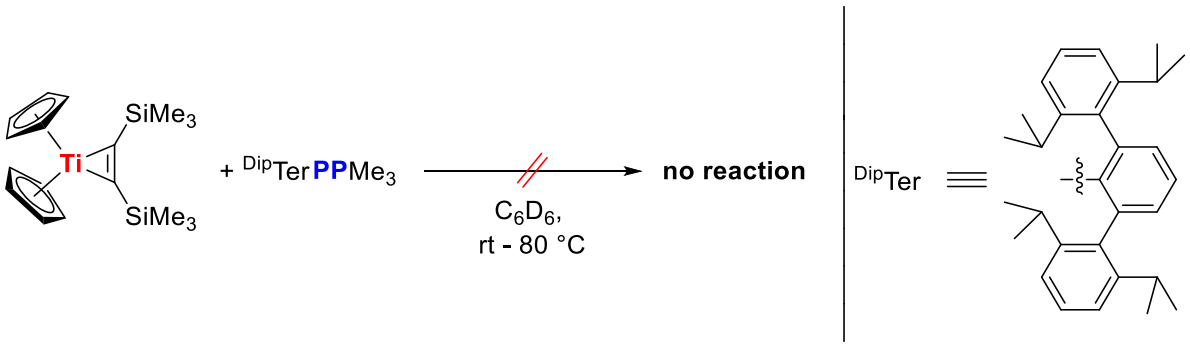

In a Young NMR tube $Cp_2Ti(btmsa)$ (**1**) (0.015 g, 0.043 mmol) and $^{Dip}TerPPMe_3$ (**2c**) (0.022 g, 0.043 mmol) were dissolved in 0.6 mL of C_6D_6. The reaction mixture was allowed to stand for 16 h at room temperature. Regular control by ^{1}H and $^{31}P\{^{1}H\}$ NMR spectroscopy showed that no reaction has occurred. Subsequent heating of the reaction mixture to 80 °C for two days and further heating to 115 °C only results in the

decomposition of $Cp_2Ti(btmsa)$ (**1**), which is shown by the release of btmsa and decreasing signal intensity for the signals of $Cp_2Ti(btmsa)$ (**1**) (Figure S8).

Figure S8: Monitoring of the reaction of $Cp_2Ti(btmsa)$ (**1**) with $^{Dipp}TerPPMe_3$ (**2c**) via ^1H NMR spectroscopy (300 MHz, C_6D_6, rt to indicated T); 0.15 ppm: btmsa, -0.32 and 6.42 ppm: $Cp_2Ti(btmsa)$ (**1**).

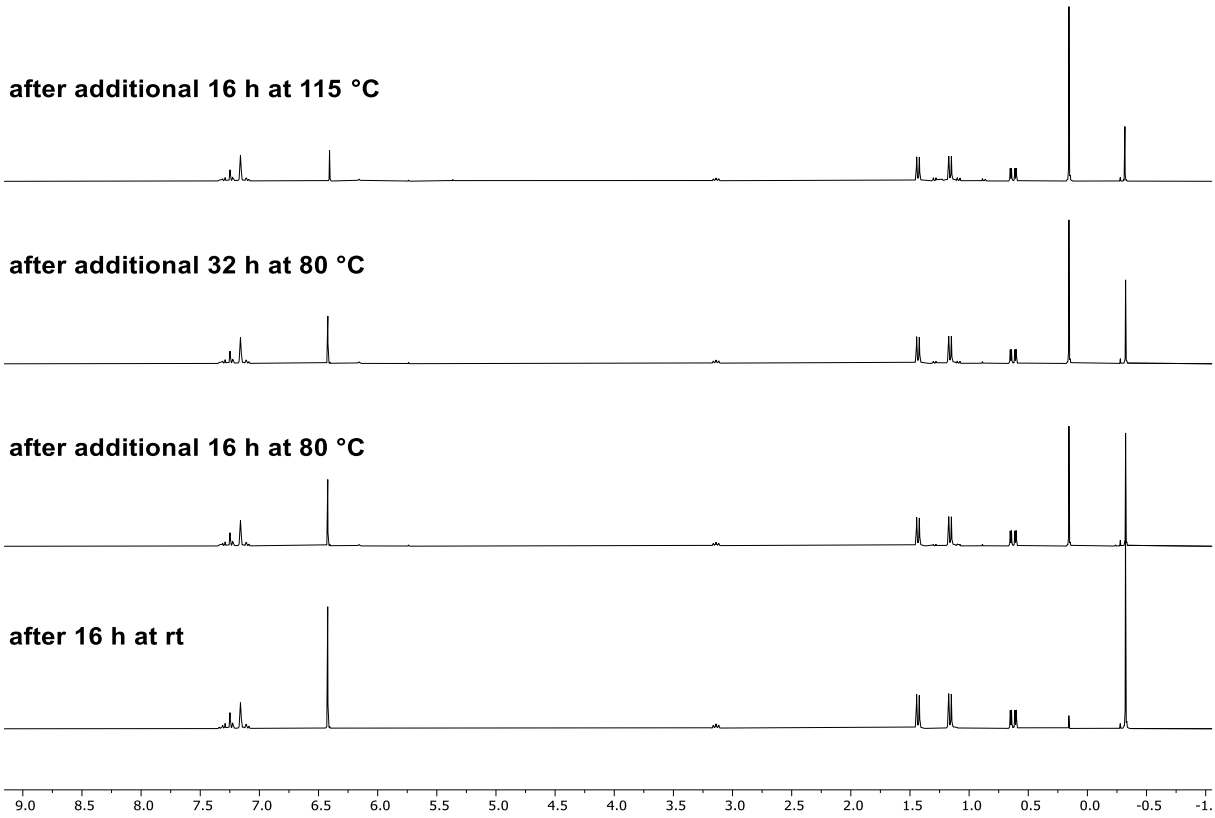

4 Syntheses of compounds

4.1 Synthesis of $Cp_2(PMe_3)TiP^{Mes}Ter$ (3)

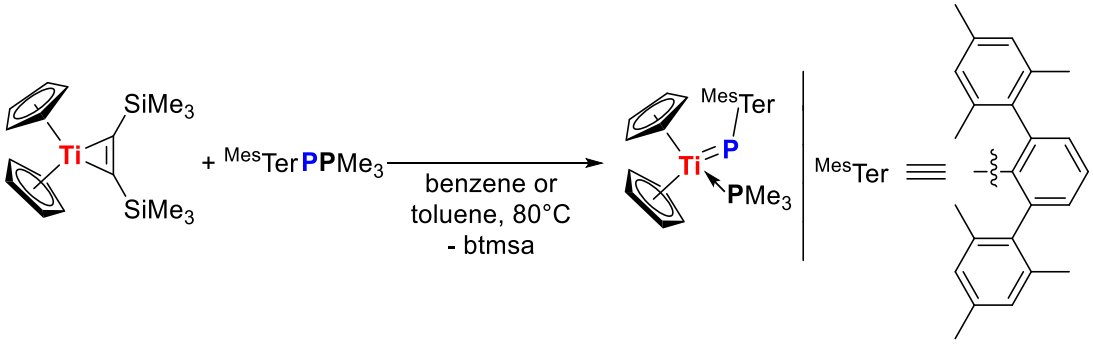

A) In a Young NMR tube $Cp_2Ti(btmsa)$ (**1**) (0.022 g, 0.063 mmol) and $^{Mes}TerPPMe_3$ (**2b**) (0.027 g, 0.063 mmol) were dissolved in either 0.6 mL of C_6D_6 or 0.6 mL of toluene-d_8. The reaction mixture was heated to 80 °C overnight, which resulted in a colour change to dark orange/red and, due to its poor solubility, precipitation of $Cp_2(PMe_3)TiP^{Mes}Ter$ (**3**). NMR spectroscopy revealed consumption of both starting materials to mainly yield $Cp_2(PMe_3)TiP^{Mes}Ter$ (**3**).

Crystals suitable for single-crystal X-ray diffraction were obtained by slowly cooling of a toluene-d_8 solution of **3** from 80°C to room temperature.

B) $Cp_2Ti(btmsa)$ (**1**) (0.331 g, 0.951 mmol) and $^{Mes}TerPPMe_3$ (**2b**) (0.400 g, 0.951 mmol) were dissolved in 10 mL of benzene and the reaction mixture was stirred for 48 h at 80 °C. All volatile components were removed under vacuum and the remaining solid was washed with small amounts of benzene (3×1 mL). Removal of all volatile components under vacuum yielded $Cp_2(PMe_3)TiP^{Mes}Ter$ (**3**) as a dark orange/red solid.

Note: **3** is poorly soluble in aromatic and aliphatic hydrocarbons such as benzene, toluene, *n*-hexane and tetrahydrofuran. Btmsa helps with the solubility so that the NMR data of attempt A are shown below.

Yield: 0.386 g (0.645 mmol; 68%).

EA: calculated: C 74.24, H 7.41; found: C 74.14, H 7.83. **^{1}H NMR** (300 MHz, C_6D_6, 298 K): δ = 0.32 (d, $^2J_{P,H}$ = 6.8 Hz, 9H, $P(CH_3)_3$), 2.20 (s(br), 6H, *p*-C*H*$_3$C$_6$H$_3$), 2-37 (s(br), 12H, *o*-C*H*$_3$C$_6$H$_3$), 5.22 (s, 5H, C_5H_5), 5.23 (s, 5H, C_5H_5), 6.42 (s, 1H, CH_{Aryl}), 6.77-6.78 (m(br), 4H, CH_{Aryl}), 7.16-7.18 (m, 2H, CH_{Aryl})* ppm. * = overlap with C_6D_5H signal. **^{13}C{^{1}H} NMR** (75 MHz, C_6D_6, 298 K): δ = 19.5 (d, $^1J_{P,C}$ = 19.8 Hz, $(PCH_3)_3$), 21.1 (*p*-$\underline{C}H_3C_6H_3$), 21.6 (*o*-$\underline{C}H_3C_6H_3$), 103.8 (C_5H_5), 114.2 (C_{Aryl}), 117.9 (C_{Aryl}), 124.5 (C_{Aryl}), 135.3 (C_{Aryl}) ppm. **Note**: All other signals are significantly broadened so that an unambiguous assignment was not possible. **^{31}P{^{1}H} NMR** (122 MHz, C_6D_6, 298 K): δ = 8.0 (d, $^2J_{P,P}$ = 21.7 Hz, $P(CH_3)_3$), 1067.3 (d, $^2J_{P,P}$ = 27.8 Hz, P^{Mes}Ter) ppm. **MS** (ESI-TOF): expected: m/z = 599.2480 $[M + H]^+$; found: m/z = 599.2484. Fragment: m/z = 523.2036 $[M + H - PMe_3]^+$.

Figure S9: ^{1}H NMR spectrum after the reaction of Cp_2Ti(btmsa) (**1**) with ^{Mes}TerPPMe$_3$ (**2b**) (procedure A) (300 MHz, C_6D_6, rt); 0.15 ppm: btmsa.

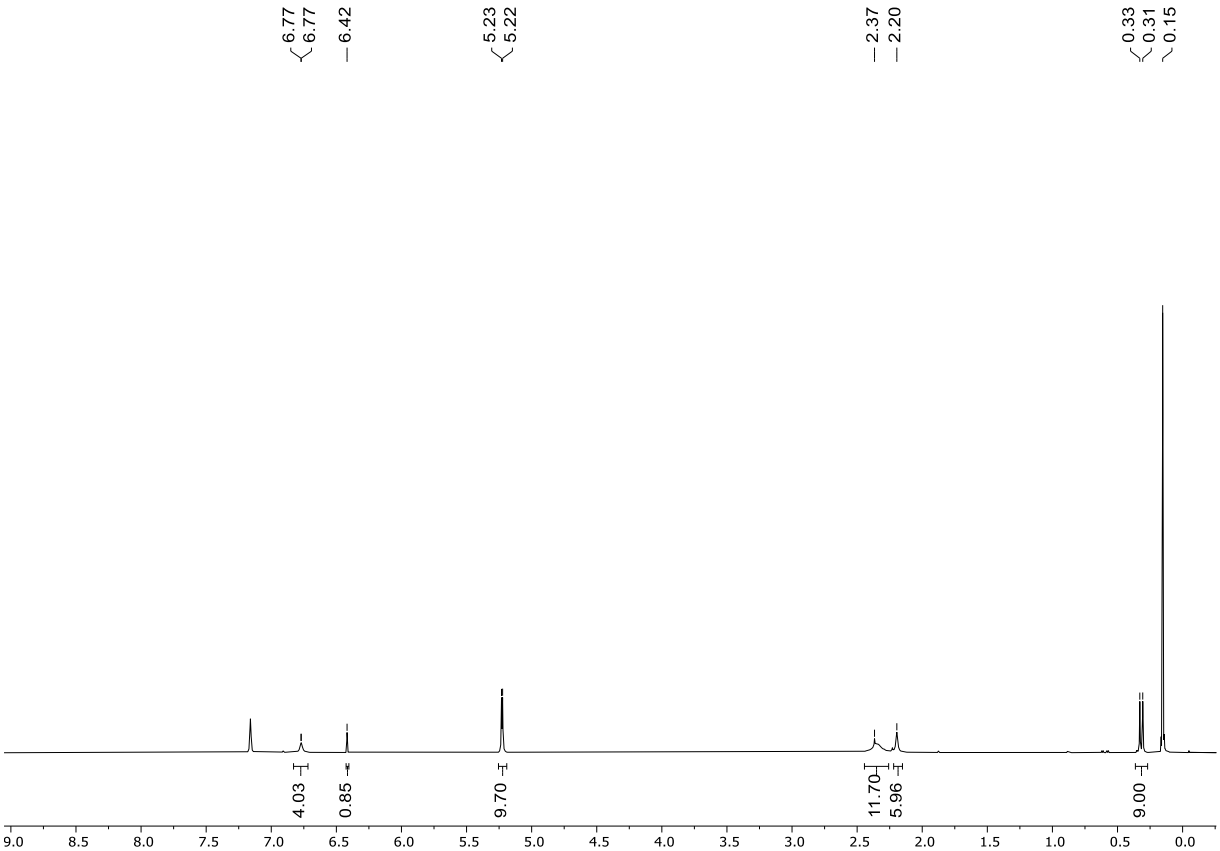

Figure S10: $^{13}C\{^1H\}$ NMR spectrum after the reaction of $Cp_2Ti(btmsa)$ (**1**) with $^{Mes}TerPPMe_3$ (**2b**) (procedure A) (75 MHz, C_6D_6, rt); 0.0 ppm: btmsa.

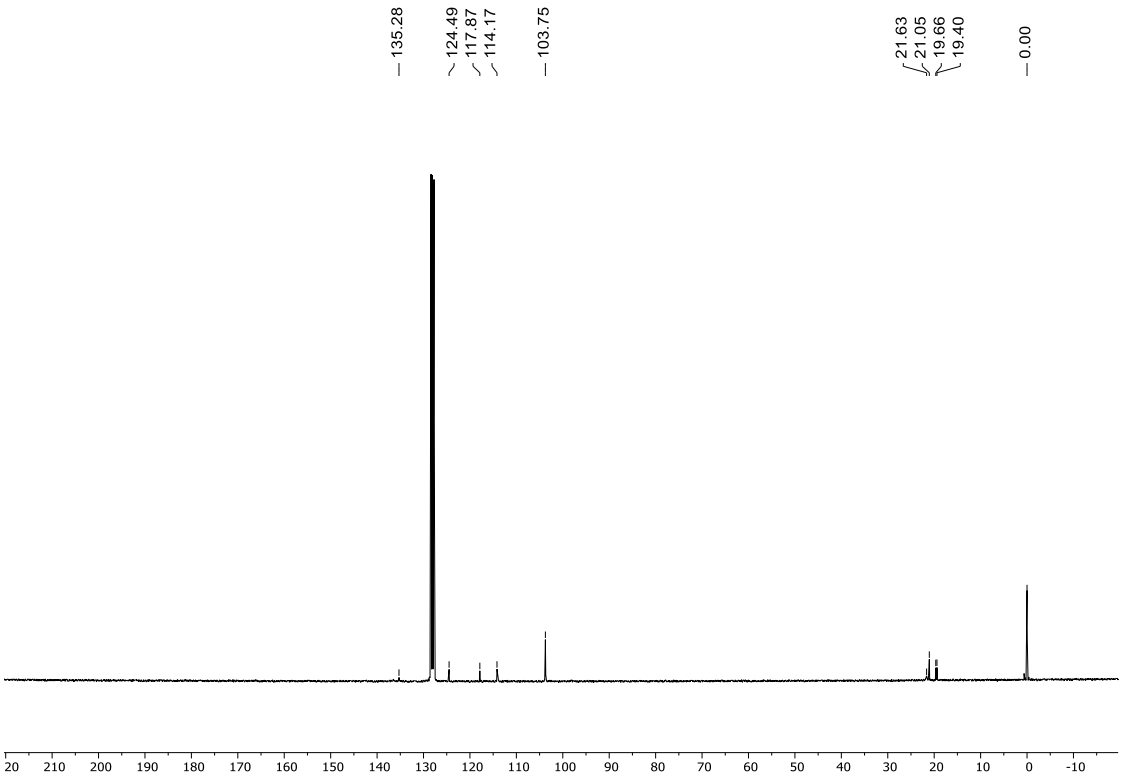

Figure S11: $^{31}P\{^1H\}$ NMR spectrum after the reaction of $Cp_2Ti(btmsa)$ (**1**) with $^{Mes}TerPPMe_3$ (**2b**) (procedure A) (122 MHz, C_6D_6, rt); #: free $^{Mes}TerP{=}PMe_3$.

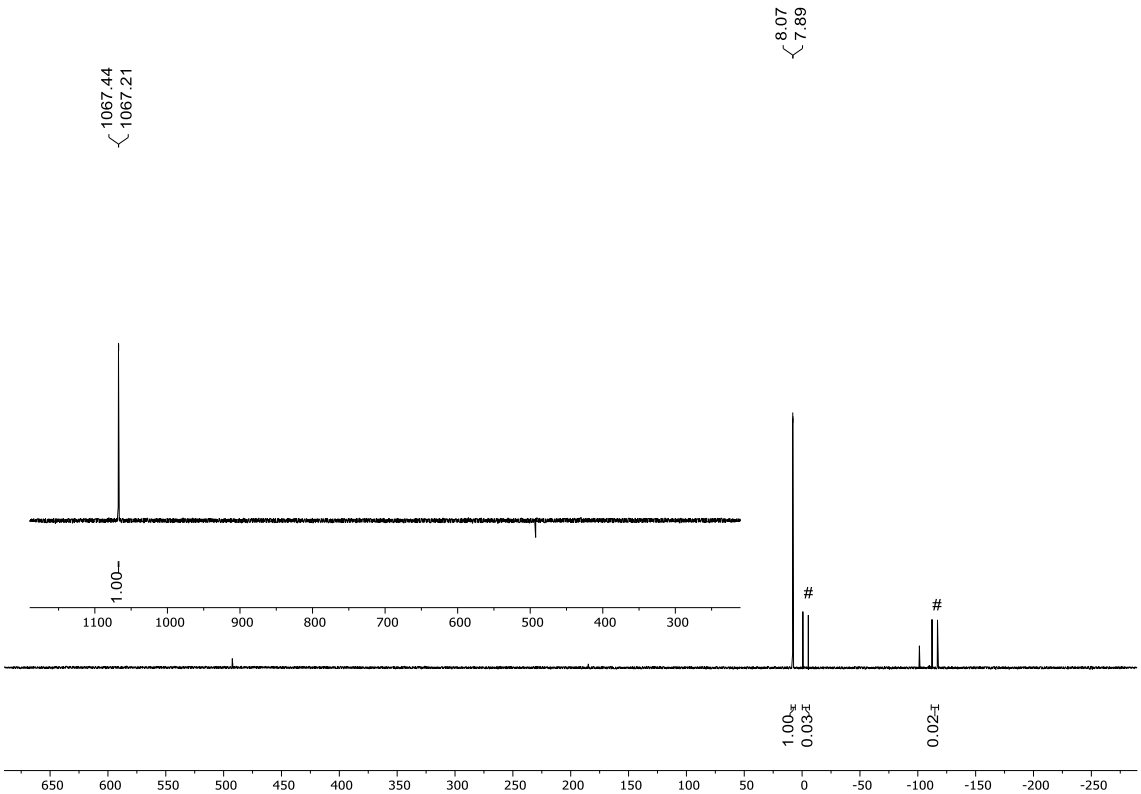

4.2 Synthesis of $Cp_2Ti(PMe_3)As^{Dip}Ter$ (5)

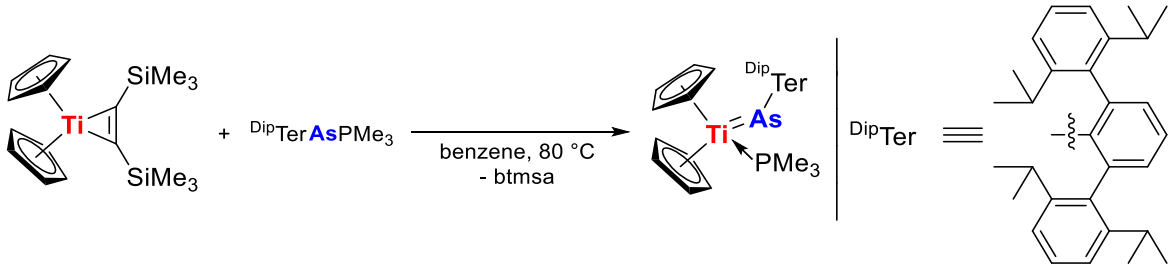

A) In a Young NMR tube $Cp_2Ti(btmsa)$ (**1**) (0.030 g, 0.086 mmol) and $^{Dip}TerAsPMe_3$ (**4**) (0.047 g, 0.086 mmol) were dissolved in 0.6 mL of C_6D_6. The reaction mixture was heated to 80 °C over night which results in a color change to dark red. All volatile components were removed under vacuum. *n*-Pentane (4×1 mL) was added to the residue and the respective supernatants were filtered through a microfiber filter.

Storage of the combined solutions at -30 °C resulted in the precipitation of crystals of **5** suitable for single crystal X-ray diffraction.

B) $Cp_2Ti(btmsa)$ (**1**) (0.019 g, 0.055 mmol) and $^{Dip}TerAsPMe_3$ (**4**) (0.030 g, 0.086 mmol) were dissolved in C_6D_6. The reaction mixture was heated to 80 °C for 16 hours which revealed complete conversion of both starting materials to give $Cp_2(PMe_3)TiAs^{Dip}Ter$ (**5**) accompanied by release of btmsa. Removal of all volatile components under vacuum gave **5** as a dark red solid.

Note: Performing the reaction at 80 °C according to procedure **B** but using an excess of $^{Dip}TerAsPMe_3$ (**4**) results in the formation of $^{Dip}TerAsAs^{Dip}Ter$ (**6**) as a byproduct (Figure S15).

Yield: 0.024 g (0.033 mmol; 60% (method **B**)).

^{1}H NMR (300 MHz, C_6D_6, 298 K): δ = 0.10 (d, $^2J_{P,H}$ = 6.6 Hz, 9H, $P(CH_3)_3$, 0.69-1.42 (m(br), 24H, $CH(CH_3)_2$), 2.42-3.80 (m(br), 4H, $CH(CH_3)_2$), 4.97-5.07 (m(br), 10H, C_5H_5), 6.86-7.05 (m(br), 5H, CH_{Aryl})*, 7.09-7.14 (m, 1H, CH_{Aryl}), 7.17-7.37 (m(br), 2H, CH_{Aryl}) ppm. * =

overlap with C_6D_5H signal. **$^{13}C\{^1H\}$ NMR** (75 MHz, C_6D_6, 298 K): δ = 19.5 (d, $^1J_{P,C}$ = 20.1 Hz, $P(CH_3)_3$) ppm. **Note**: All other signals are significantly broadened so that a clear assignment was not possible. **$^{31}P\{^1H\}$ NMR** (122 MHz, C_6D_6, 298 K): δ = 16.7 ppm.

Figure S12: ^{1}H NMR spectrum after the reaction of $Cp_2Ti(btmsa)$ (**1**) with $^{Dip}TerAsPMe_3$ (**4**) (300 MHz, C_6D_6, rt).

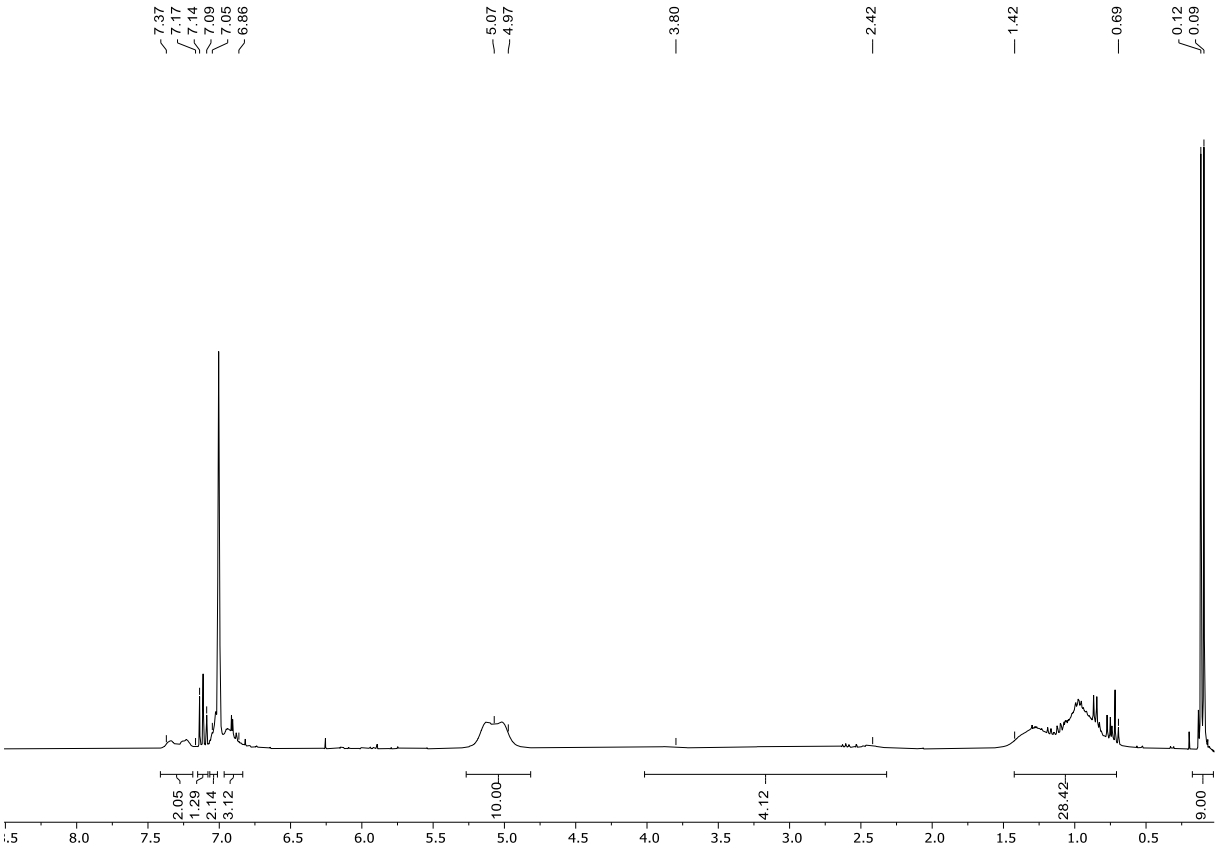

Figure S13: ^{13}C NMR spectrum after the reaction of $Cp_2Ti(btmsa)$ (**1**) with $^{Dip}TerAsPMe_3$ (**4**) (122 MHz, C_6D_6, rt).

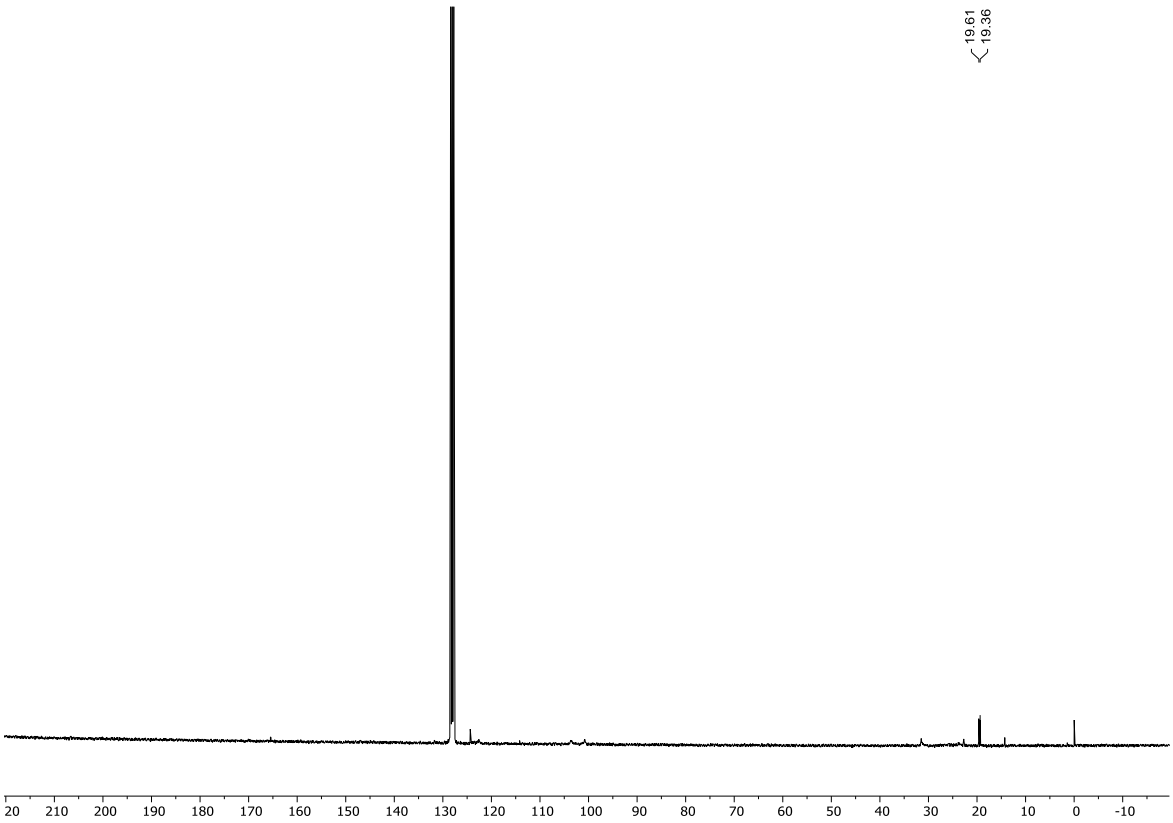

Figure S14: $^{31}P\{^1H\}$ NMR spectrum after the reaction of $Cp_2Ti(btmsa)$ (**1**) with $^{Dip}TerAsPMe_3$ (**4**) (122 MHz, C_6D_6, rt).

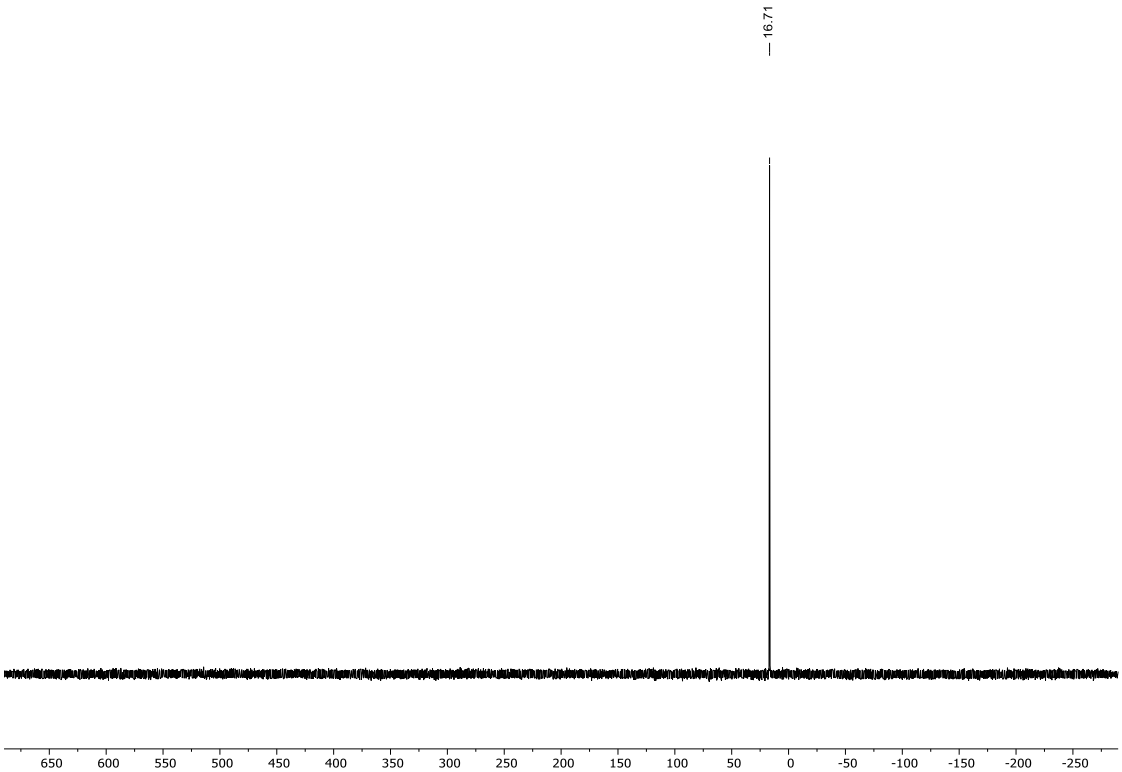

Figure S15: ^{1}H NMR spectrum of the reaction of excess ^{Dip}TerAsPMe$_3$ (**4**) with Cp$_2$Ti(btmsa) (**1**) (300 MHz, C_6D_6, rt) * = characteristic signals of ^{Dip}TerAsAs^{Dip}Ter (**6**), + = characteristic signals of ^{Dip}TerAsPMe$_3$ (**4**).

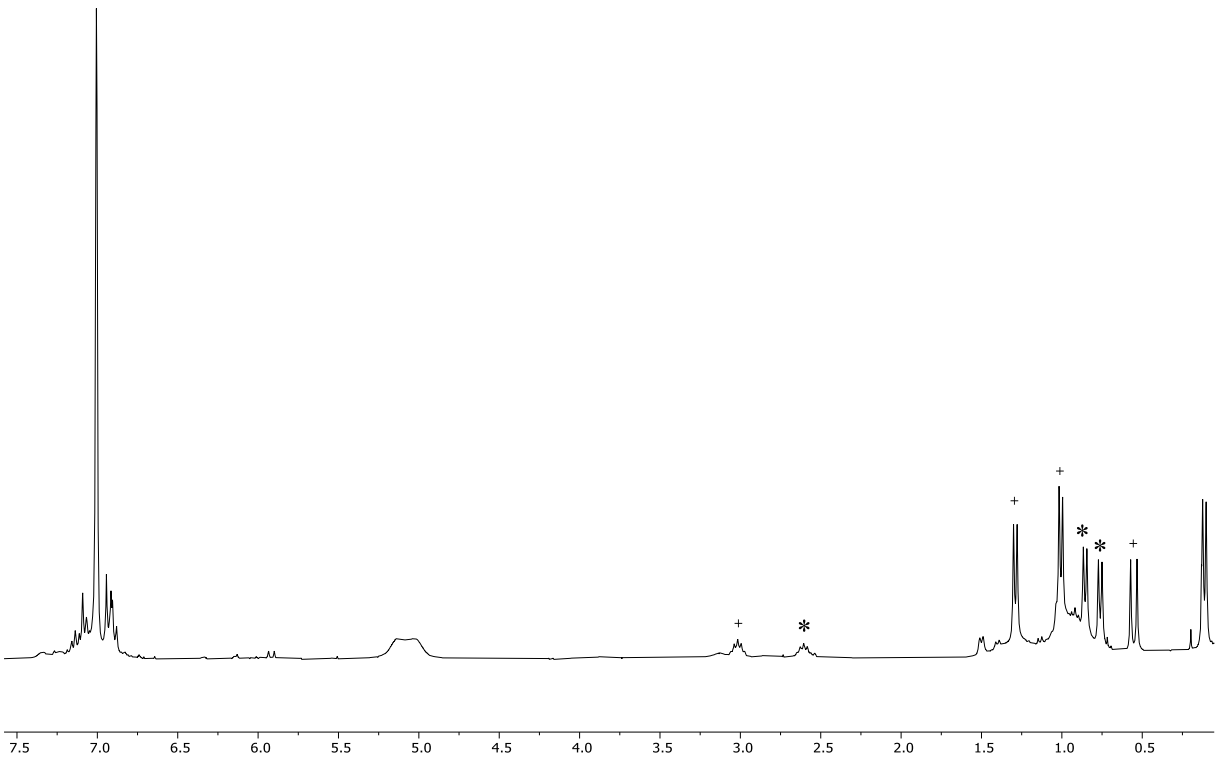

4.3 Synthesis of (^{Dip}TerAs)$_2$ (6)

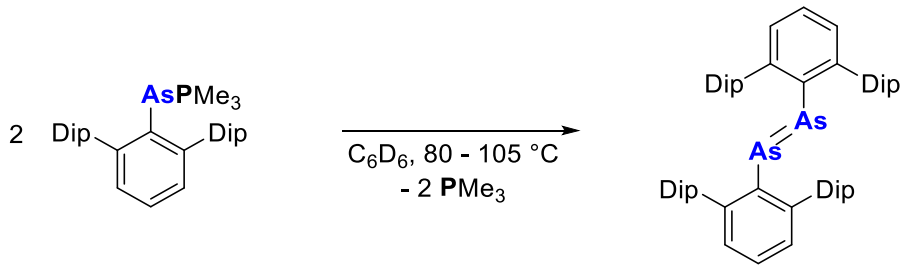

In a Young NMR tube ^{Dipp}TerAsPMe$_3$ (**4**) (0.030 g, 0.055 mmol) was dissolved in 0.6 mL of C_6D_6. The sample was heated to 80 °C for 7 hours and subsequent ^{1}H and ^{31}P{^{1}H} NMR spectroscopy revealed slow conversion of **4**. Therefore, the temperature was increased to 105 °C, and the sample was regularly analysed by ^{1}H and ^{31}P{^{1}H} NMR spectroscopy. After 130 h at that temperature **4** was consumed completely to give ^{Dip}TerAsAs^{Dip}Ter (**6**). All volatile components were removed under vacuum. 2 mL of

n-pentane were added, the solution was passed through a microfiber filter, and stored at -30 °C to yield ^{Dip}TerAsAs^{Dip}Ter (**6**) as an orange crystalline solid. These crystals were suitable for single crystal X-ray diffraction. Crystals suitable for single crystal X-ray diffraction were also obtained from a saturated solution of **6** in C_6D_6 at room temperature.

Yield: 0.014 g (0.015 mmol; 54%).

^{1}H NMR (300 MHz, C_6D_6, 298 K): δ = 0.92 (d, $^3J_{H,H}$ = 6.8 Hz, 24H, CH(C*H*$_3$)$_2$), 1.02 (d, $^3J_{H,H}$ = 6.9 Hz, 24H, CH(C*H*$_3$)$_2$), 2.77 (hept, $^3J_{H,H}$ = 7.0 Hz, 8H, C*H*(CH$_3$)$_2$), 7.04-7.05 (m, 4H, CH$_{Aryl}$), 7.07-7.08 (m, 10H, CH$_{Aryl}$), 7.17-7.21 (m, 4H, CH$_{Aryl}$)* ppm. * = overlap with C_6D_5H signal. **^{13}C{^{1}H} NMR** (75 MHz, C_6D_6, 298 K): δ = 23.8 (CH(<u>C</u>H$_3$)$_2$), 25.8 (CH(<u>C</u>H$_3$)$_2$), 31.1 (<u>C</u>H(CH$_3$)$_2$), 123.8 (CH$_{Aryl}$), 128.2 (CH$_{Aryl}$)*, 128.9 (CH$_{Aryl}$), 130.8 (CH$_{Aryl}$), 140.4 (C$_{q,Aryl}$), 144.9 (C$_{q,Aryl}$), 146.2 (C$_{q,Aryl}$), 151.4 (C$_{q,Aryl}$) ppm. * = overlap with C_6D_6 signal. **MS** (ESI-TOF): expected: m/z = 945.4301 [M + H]$^+$, 967.4114 [M + Na]$^+$; found: m/z = 945.4283 [M + H]$^+$, 967.4113 [M + Na]$^+$.

Figure S16: Monitoring of ^{Dip}TerAsPMe$_3$ (**4**) at higher temperatures via ^{1}H NMR spectroscopy (300 MHz, C_6D_6).

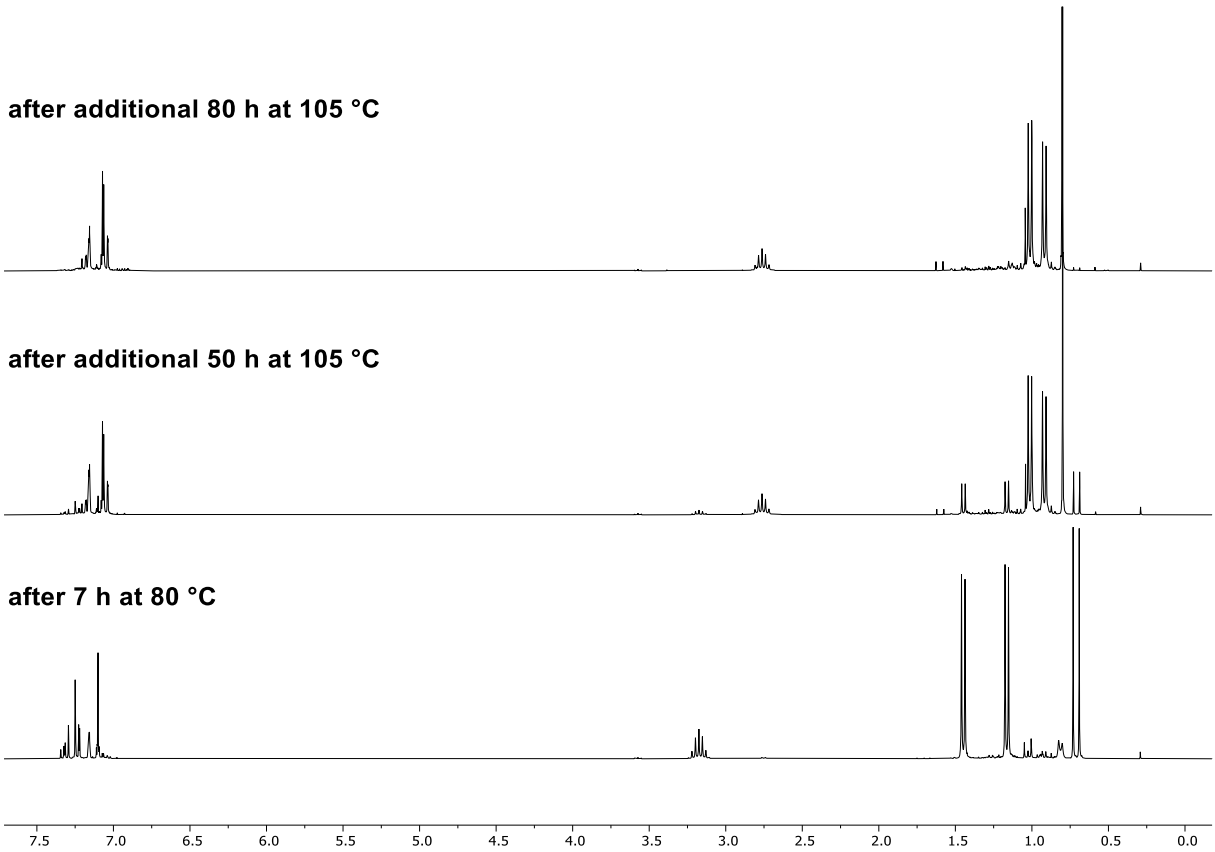

Figure S17: Monitoring of ^{Dip}TerAsPMe$_3$ (4) at higher temperatures via ^{31}P{^{1}H} NMR spectroscopy (122 MHz, C_6D_6, rt); -14.6 ppm: ^{Dip}TerAsPMe$_3$ (6); -57.6 ppm: PMe$_3$.

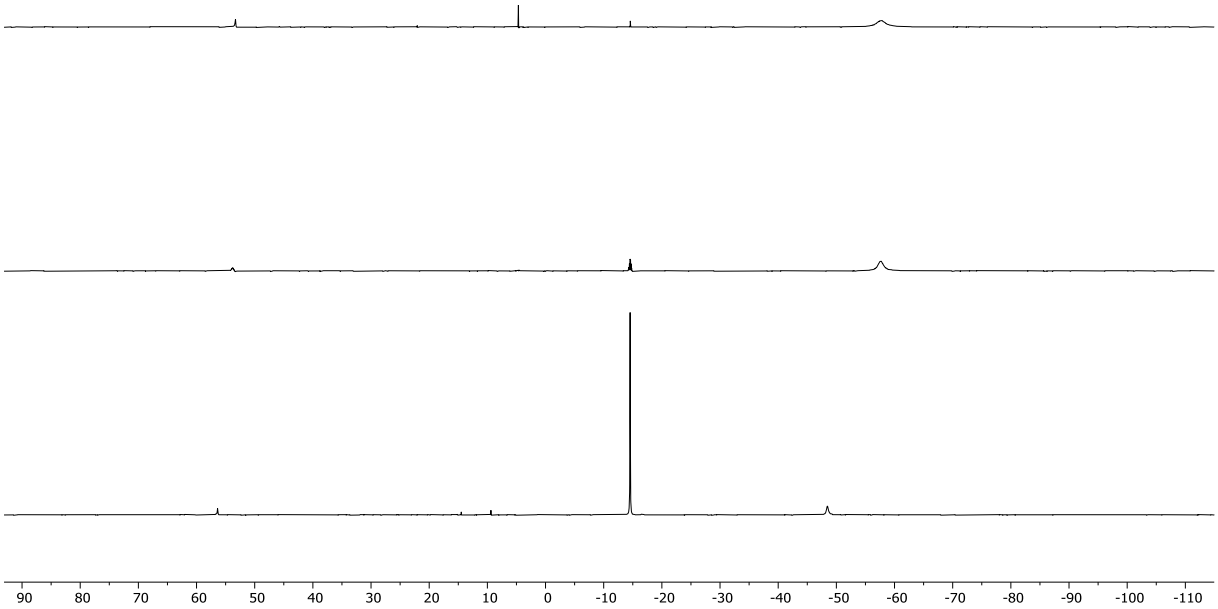

Figure S18: ^{1}H NMR spectrum of ^{Dip}TerAsAs^{Dip}Ter (**6**) (300 MHz, C_6D_6, rt); 0.29 ppm: silicon grease.

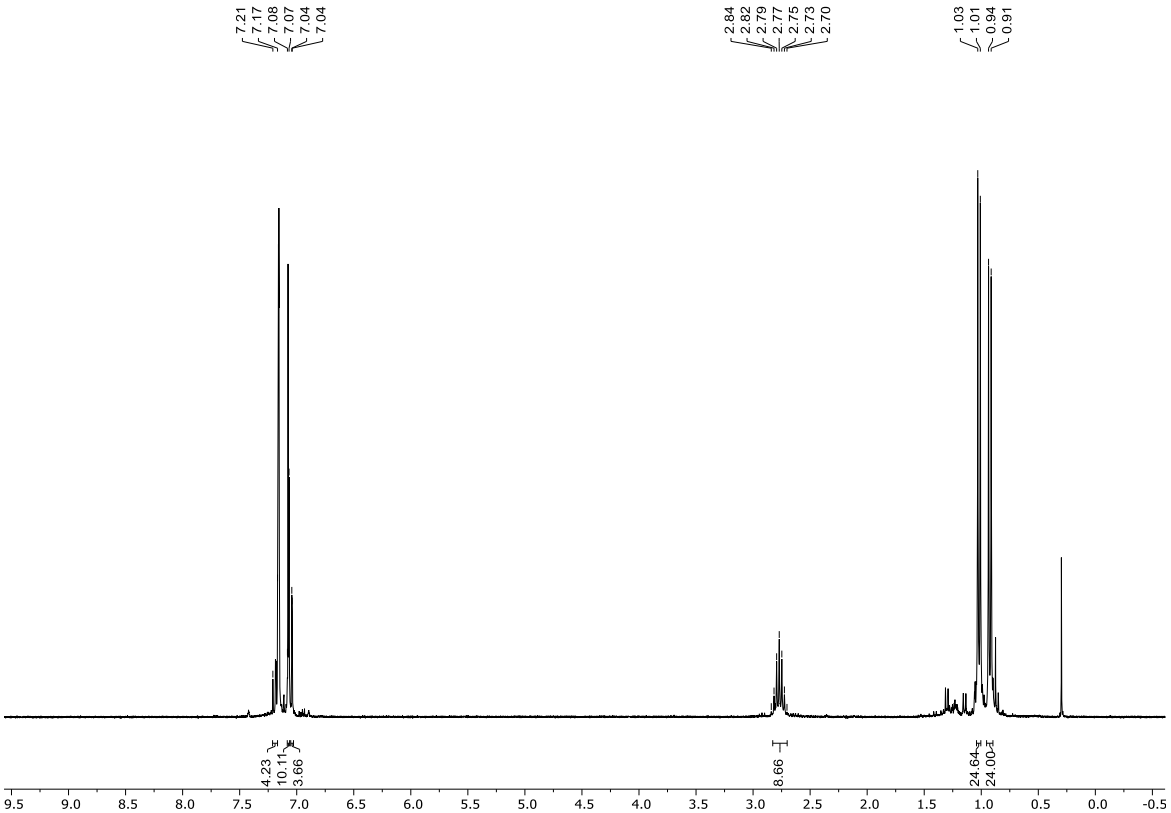

Figure S19: ^{13}C{^{1}H} NMR spectrum of ^{Dip}TerAsAs^{Dip}Ter (**6**) (75 MHz, C_6D_6, rt); 1.4 ppm: silicon grease.

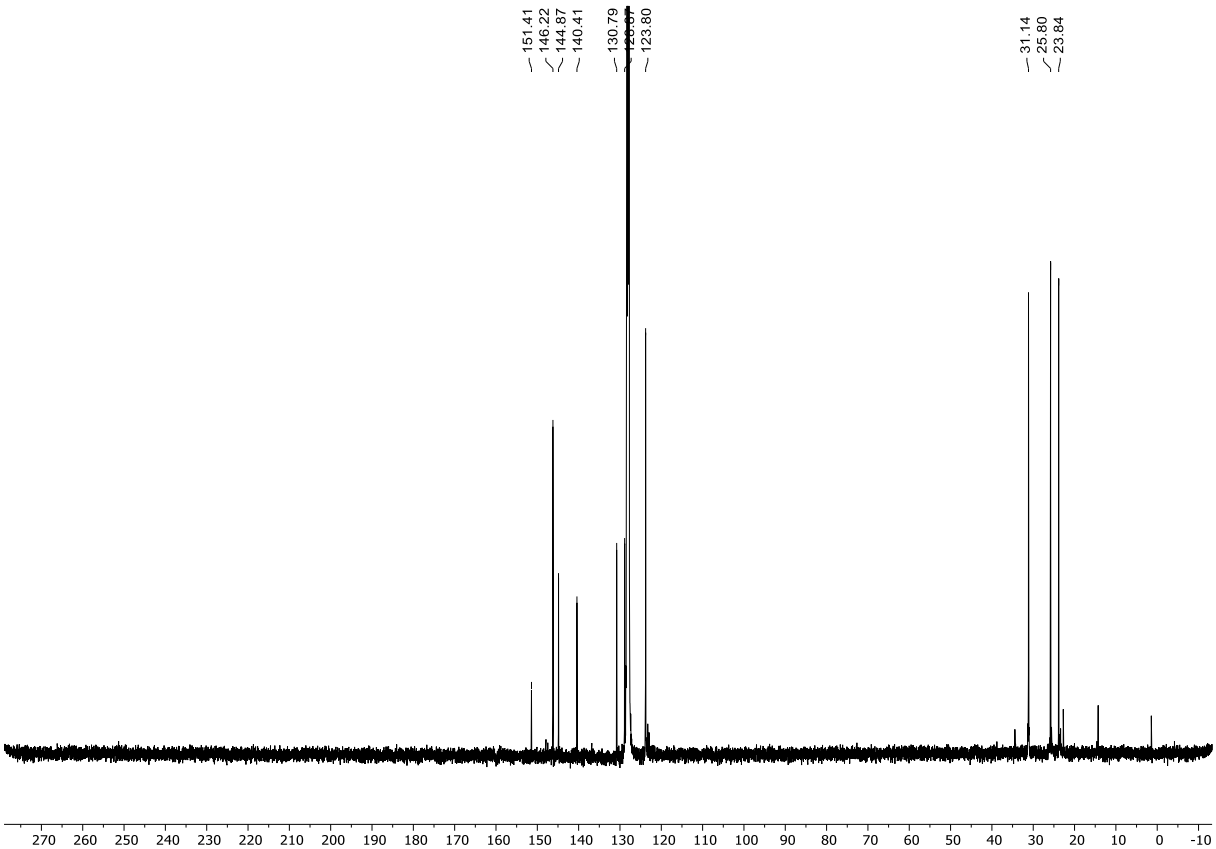

5 Computational details

5.1 General remarks

Computations were carried out using *Gaussian16*[8] and the standalone version of *NBO 6.0*.[9]

In a first step we investigated the thermodynamic feasibility of the reaction between group 4 alkyne complexes and experimentally accessible phospha- as well as arsa-Wittig reagents to form the respective phosphinidene or arsinidene complexes of the type $Cp_2M(PMe_3)PAr$ (M = Ti, Zr). Therefore, we optimized the real-size molecules using the hybrid density functional method B3LYP,[10,11] in combination with the basis set def2svpp,[12] and the empirical dispersion correction GD3BJ[13] (notation: B3LYP/GD3BJ/def2svpp). Vibrational frequencies were also computed, to include zero-point vibrational energies in thermodynamic parameters and to characterise all structures as minima on the potential energy surface. NLMO analyses were performed using the standalone version of NBO 6.0. QT-AIM, ELF and Wiberg Bondindex calculations/visualization were performed using MultiWfn 3.6 employing *Gaussian16* formatted checkpoint files.[14] For the visualization of 3D-quantum chemical results we used GaussView6.1.1.[15] In addition to the electronic supporting information we provide a multi-structure xyz-file including all calculated molecules.

Please note that all computations were carried out for single, isolated molecules in the gas phase (ideal gas approximation). There may well be significant differences between gas phase and condensed phase.

5.2 Thermochemistry

In this chapter we summarize the results of our thermodynamic calculations, which were performed on the B3LYP/GD3BJ/def2svpp level of theory as described

beforehand. It should be noted that we did not calculate transition states or intermediate structures for further insights into the reaction mechanism. Nevertheless, this simple thermodynamic consideration nicely supports the observed reaction behaviours.

5.2.1 Group 4 metallocenes bearing phosphinidenes and arsinidenes

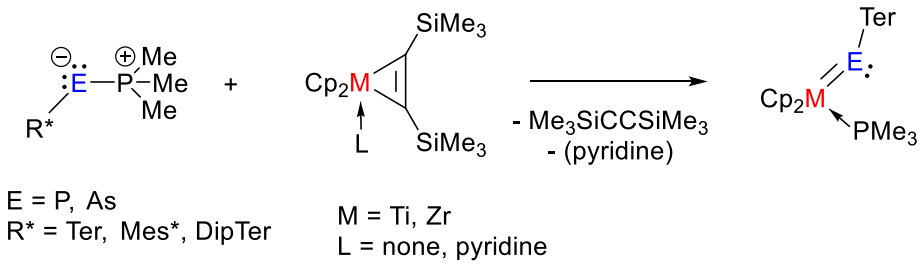

***Scheme S1*:** Calculated reaction sequence to group 4 metallocenes bearing phosphinidenes and arsinidenes.

Table S4. Summary of calculated thermodynamic values for the formation of group 4 metallocene bearing phosphinidenes and arsinidenes.

Compound	$\Delta_R H$ [kJ/mol]	$\Delta_R G$ [kJ/mol]	$\Delta_R H$ [kcal/mol]	$\Delta_R G$ [kcal/mol]
$Cp_2Ti(PMe_3)P^{Mes}Ter$	-54.7	-47.0	-13.1	-11.2
$Cp_2Ti(PMe_3)P^{Dip}Ter$	-48.0	-37.8	-11.5	-9.0
$Cp_2Ti(PMe_3)PMes^*$	-27.8	-24.1	-6.6	-5.8
$Cp_2Zr(PMe_3)P^{Mes}Ter$	16.2	-38.8	3.9	-9.3
$Cp_2Ti(PMe_3)As^{Mes}Ter$	-62.1	-56.3	-14.9	-13.4
$Cp_2Zr(PMe_3)As^{Mes}Ter$	13.6	-39.4	3.3	-9.4
$Cp_2Ti(PMe_3)As^{Dip}Ter$	-57.6	-49.6	-13.8	-11.8
$Cp_2Zr(PMe_3)As^{Dip}Ter$	20.8	-33.9	5.0	-8.1

5.2.2 Decomposition of phospha-Wittig reagents to formal CH activation products

As outlined in Section 3 of the SI in the case of Mes*- and ^{Dip}Ter-substituted phospha-Wittig reagents no conversion to the desired titanocene phosphinidenes was observed.

In case of the Mes* phospha-Wittig reagent **2a** instead the clean conversion into a phosphaindane species was detected. The thermodynamic values for this formal CH-activation process on a CH group of the sterically loaded substituent clearly show this step, in the case of the Mes* substituent, to be the thermodynamically preferred compared to the formation of the phosphinidene complex. Furthermore, the endothermic reaction enthalpies in case of the ^{Mes}Ter- and ^{Dip}Ter-derivatives explain the absence of analogous decomposition reactions.

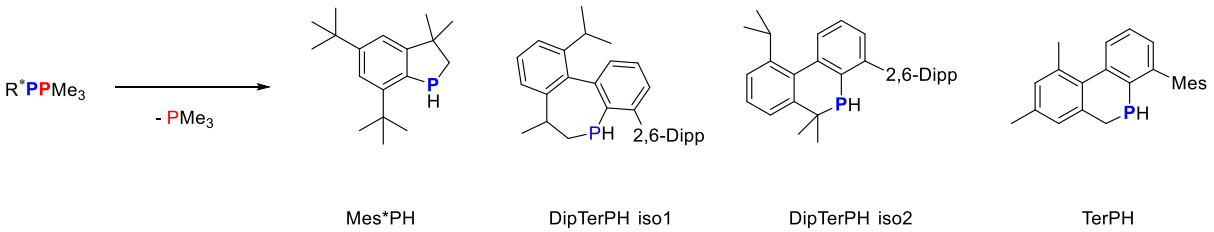

***Scheme S2*:** Calculated reaction sequence to formal CH-activation products.

Table S5. Summary of calculated thermodynamic values for the formation of formal CH activation products.

Compound	Δ_RH [kJ/mol]	Δ_RG [kJ/mol]	Δ_RH [kcal/mol]	Δ_RG [kcal/mol]
^{Mes}TerPH	1.7	−45.0	0.4	−10.7
^{Dip}TerPH iso1	5.4	−42.2	1.3	−10.1
^{Dip}TerPH iso2	9.5	−39.9	2.3	−9.5
Mes*PH	−66.4	−116.5	−15.9	−27.9

5.2.3 Report of total enthalpies and energies for all calculated molecules

Table S6. Summary of thermodynamic data of all calculated compounds, if different isomers were considered only the minimum isomer (marked with *) was used for thermodynamic calculations.

Compound	Nimag	HF	ZPE [kcal/mol]	H_{tot} [a.u.]	G_{tot} [a.u.]
H_2	0	-1.1710938	6.211710	-1.157890	-1.172736
$C_2(SiMe_3)_2$	0	-894.3438671	145.050420	-894.094213	-894.159269
PMe_3	0	-460.9178429	70.239730	-460.798299	-460.834131

pyridine	0	-248.111213	55.723280	-248.017208	-248.049810
^{Mes}TerPH	0	-1270.310053	261.540350	-1269.868360	-1269.948021
^{Dip}TerPH iso1	0	-1506.022004	369.933810	-1505.400794	-1505.492960
^{Dip}TerPH iso2	0	-1506.019420	369.098070	-1505.399231	-1505.492091
Mes*PH	0	-1044.194176	267.013690	-1043.746549	-1043.816315
$Cp_2Ti(C_2(SiMe_3)_2)$	0	-2130.617297	251.521230	-2130.187530	-2130.275546
$Cp_2Zr(C_2(SiMe_3)_2)$py	0	-1576.468978	308.366770	-1575.942928	-1576.042481
^{Mes}TerPPMe$_3$	0	-1731.2328654	333.781820	-1730.667291	-1730.765023
^{Dip}TerPPMe$_3$	0	-1966.946423	442.40777	-1966.201131	-1966.311015
Mes*PPMe$_3$	0	-1505.091645	340.16317	-1504.519546	-1504.606055
^{Mes}TerAsPMe$_3$	0	-3625.6173707	333.075840	-3625.052389	-3625.151929
^{Dip}TerAsPMe$_3$	0	-3861.33058	441.73408	-3860.585878	-3860.69717
$Cp_2Ti(PMe_3)P^{Mes}$Ter iso1	0	-2967.5287754	441.445210	-2966.781450	-2966.899194
$Cp_2Ti(PMe_3)P^{Mes}$Ter iso2	0	-2967.5287754	441.445220	-2966.781450	-2966.899194
$Cp_2Ti(PMe_3)P^{Mes}$Ter trip on sin geom sp	2	-2967.4892274	440.593330	-2966.744298	-2966.861182
$Cp_2Ti(PMe_3)^{Mes}$PTer trip opt	0	-2967.5152634	440.920400	-2966.768276	-2966.888126
$Cp_2Ti(PMe_3)P^{Dip}$Ter	0	-3203.240121	550.34371	-3202.31272	-3202.441707
$Cp_2Ti(PMe_3)$PMes*	0	-2741.377354	447.6102	-2740.623446	-2740.731506
$Cp_2Zr(PMe_3)P^{Mes}$Ter	0	-2165.2388170	440.25904	-2164.492634	-2164.613202
$Cp_2Ti(PMe_3)As^{Mes}$Ter	0	-4861.916139	440.76626	-4861.169376	-4861.289636
$Cp_2Zr(PMe_3)As^{Mes}$Ter	0	-4059.6244079	439.69117	-4058.878697	-4059.000337
$Cp_2Ti(PMe_3)As^{Dip}$Ter 01	0	-5097.627992	549.63502	-5096.701148	-5096.832328
$Cp_2Ti(PMe_3)As^{Dip}$Ter trip opt	0	-5097.6146257	548.40668	-5096.688912	-5096.824735
$Cp_2Ti(PMe_3)As^{Dip}$Ter TS	1	-5097.6013088	548.96615	-5096.675722	-5096.807185
$Cp_2Ti(PMe_3)As^{Dip}$Ter -1(Charge) 2 (Mult)	0	-5097.6504725	546.29912	-5096.727902	-5096.863079
$Cp_2Zr(PMe_3)As^{Dip}$Ter	0	-4295.335088	548.41375	-4294.409468	-4294.543496
$Cp_2Ti(PMe_3)As^{Dip}$Ter iso2	0	-5097.620866	549.66600	-5096.694069	-5096.824913
$Cp_2Ti(PMe_3)^{Mes}$PTer iso2	0	-2969.5267313	441.27406	-2968.779323	-2968.898715
$Cp_2Ti(PMe_3)P^{Mes}$Ter trip on sin geom sp	2	-2969.4862653	440.53012	-2968.741222	-2968.858093
Cp2Ti$(PMe_3)^{Mes}$PTer iso3 "TS Ter rot" sp	0	-2969.4964196	439.29505	-2968.756001	-2968.862061

Cp2Ti(PMe$_3$)As^{Dip}Ter	0	-5100.0683280	549.61907	-5099.141199	-5099.273392
Cp2Ti(PMe$_3$)As^{Dip}Ter_ trip on sin geom sp	1	-5100.0315314	549.07103	-5099.105687	-5099.2391
Complex II singlet opt	0	-3331.8877943	762.2345	-3330.605817	-3330.770986
Complex II triplet sp		Did not converged			
Complex III singlet opt	0	-3419.5232041	630.65398	-3418.461361	-3418.602137
Complex III triplet sp	2	-3419.4770355	629.60201	-3418.417837	-3418.557335
Complex IV singlet opt	0	-2167.1455579	439.98482	-2166.399405	-2166.52218
Complex IV triplet sp	3	-2167.0884977	438.92127	-2166.345958	-2166.464271
Complex V singlet opt	0	-2354.539857	399.7258	-2353.861838	-2353.976107
Complex V triplet sp	6	-2354.458006	396.44008	-2353.788477	-2353.895104
Complex II singlet svp on tzvp structure	29	-3329.151259	761.78629	-3327.88572	-3328.017315
Complex II triplet sp	30	-3329.10444	760.54984	-3327.840953	-3327.974888

5.3 Bonding analysis of Cp$_2$Ti(PMe$_3$)P^{Mes}Ter (3) and Cp$_2$Ti(PMe$_3$)As^{Dip}Ter (5)

In this chapter, we summarize the most important results from a series of different bonding analyses to gain a deeper insight into the electronic situation of the respective phosphinidine (**3**) and arsinidene (**5**) complexes. These calculations were performed on the molecular structures optimized at B3LYP/GD3BJ/def2tzvp level of theory. To verify the chosen method, we compared selected bond parameters with the metrical parameters obtained by single crystal X-Ray crystallography.

Table S7. Deviations of the calculated structures from the experimental molecular structure of Cp$_2$Ti(PMe$_3$)PTer (**3**).

Bonding parameter	SC-XRD	B3LYP/GD3BJ/def2svpp		B3LYP/GD3BJ/def2tzvp	
Ti-PMe3	2.569	2.550	-0.019	2.552	-0.017
Ti-PTer	2.423	2.334	-0.089	2.335	-0.088

P-CTer	1.842	1.852	0.010	1.842	0.000
P-Ti-P	86.820	88.940	2.120	89.650	2.830
Ti-P-CTer	122.110	123.590	1.480	124.420	2.310
P-Ti-P-CTer	-119.710	-116.490	3.220	-115.520	4.190

Table S8. Deviations of the calculated structures from the experimental molecular structure of $Cp_2Ti(PMe_3)As^{Dip}Ter$ (**5**) (For this analysis, we compare only the values of the best resolved molecule 1 among the three independent experimentally determined, Figure S2).

Bonding parameter	SC-XRD	01/B3LYP/GD3BJ/def2svpp		01/B3LYP/GD3BJ/def2tzvp	
Ti-PMe3	2.555	2.545	-0.010	2.546	-0.009
Ti-AsDipTer	2.473	2.441	-0.032	2.446	-0.027
As-CDipTer	1.989	1.994	0.005	1.992	0.003
P-Ti-As	88.05	87.27	-0.78	87.53	-0.52
Ti-As-CDipTer	121.73	119.99	-1.74	120.68	-1.05
P-Ti-As-CDipTer	115.20	115.04	-0.16	115.01	-0.19

Table S9. Deviations of the calculated structures from the experimental molecular structure of $^{Dip}TerAsAs^{Dip}Ter$ (**6_i**).

Bonding parameter	SC-XRD	01/B3LYP/GD3BJ/def2svpp		01C2h/B3LYP/GD3BJ/def2svp	
As-As	2.268	2.271	0.003	2.272	0.004
As-C	1.990	2.005	0.015	2.005	0.015
C-As-As	101.150	101.660	0.510	101.660	0.510
As-C-C	120.890	120.310	-0.580	120.310	-0.580
C-As-As-C	180.000	180.000	0.000	180.000	0.000
C-C-As-As	95.730	95.420	-0.310	95.140	-0.590

We found two different energetically identical isomers of $Cp_2Ti(PMe_3)P^{Mes}Ter$ (**3**), which can be transformed into each other by rotation of the sterically demanding terphenyl substituent around the P−C axis. In the case of $Cp_2Ti(PMe_3)As^{Dip}Ter$ (**5**) we found two energetically different but similar isomers, which can be transferred via an formal swing through of the arsinidene into each other. The activation barrier of the isomerisation in the case of **5** is significant lower compared to that of **3**, which might give an explanation for the broader resonances in the NMR spectra of compound **5**.

Table S10. Summary of calculated thermodynamic values for a rotation of the terphenyl ligand around the P−C axis.

Rotational Barrier	$\Delta_R H$ [kJ/mol]	$\Delta_R G$ [kJ/mol]	$\Delta_R H$ [kcal/mol]	$\Delta_R G$ [kcal/mol]
$Cp_2Ti(PMe_3)P^{Mes}Ter$ "TS Ter rot" sp	61.2	96.2	14.6	23.0
Cp2Ti_AsDipTer_PMe3 "TS DipTer swing through"	66.8	66.0	16.0	15.8

5.3.1 NBO analysis and Natural Molecular Orbitals NLMOs of 3 and 5.

NBO6.0 analyses of the B3LYP/GD3BJ/def2tzvp optimized structures of **3** and **5** were performed to analyse the natural localized molecular orbitals (NLMO). The NBO routine found a double bond between P(82) and Ti(84) in **3**, in agreement with the Lewis structure in Scheme S1. It is worth to note that this π-type NBO as well as the LP at P(82) are only occupied by approx. 1.8 electrons. At this point it should be mentioned that the occupations in arsinidene complex **5** behave in a similar way. This could be in general an indicator for a delocalized double bond or for a biradical character of the Ti=P or Ti=As bonds (as outlined earlier), which is not well represented in the NBO picture. Based on this theory, the condensed NLMO analyses (listed below) clearly characterizes the Ti(84)-P(83)Me_3 bond as a dative bond, with a major contribution (74%) of sp-hybrid orbitals at the phosphorus atom. We found two different types of Ti(84)-P(82) bonds in agreement with the double bond character. The Ti-P σ-bond mainly consists of sp^3 type hybrid at phosphorus and a d-type orbital at the titanium center with small s orbital contributions. This Ti(84)-P(82) NLMO shows only small contributions from the carbon atom of the terphenyl substituent (1.34 %). The second Ti(84)-P(82) NLMO is best described as a π-type Ti=P bond consisting of pure p orbital at phosphorus and pure d orbital character at the titanium center. This Ti(84)-P(82) NLMO shows only small contributions from the phosphorus atom of the PMe_3 ligand (1.35 %). Furthermore, the lone pair (LP) at the phosphinidene phosphorus is best described as sp-hybrid orbital.

When evaluating the NLMO's of the arsinidene complex $Cp_2Ti(PMe_3)As^{Dip}Ter$ (**5**), it is immediately noticeable that the natural localized bonding orbitals described here are very similar to those of the lighter phosphinidene derivative **3**. Furthermore, it is noticeable that no remarkable contributions of the adjacent carbon atoms are found (threshold value > 1.3%). A closer look reveals only small differences in the hybridization of the arsenic lone pair with a $sp^{0.5}$ hybridization compared to the sp hybrid on the phosphinidene P atom as well as the sp^4 hybrid on As in the Ti-As σ-bond compared to the sp^3 hybrid on the comparable P atom.

Table S11. Summary of selected NLMO's of $Cp_2Ti(PMe_3)^{Mes}PTer$ (**3**).

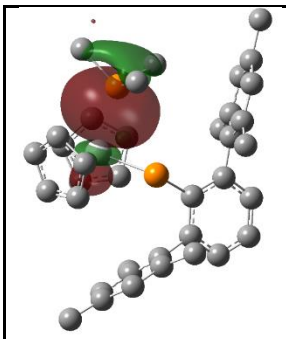	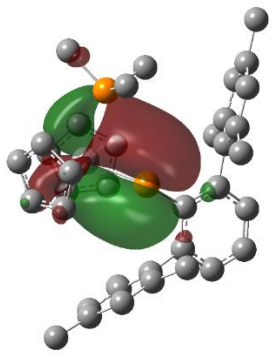
Shortened NLMO Analysis of Ti(84)-P(83)Me_3 σ-bond (threshold > 1.3%) 159. (2.00000) 96.7058% BD (1) P 83-Ti 84 73.856% P 83 s(45.08%)p 1.21(54.77%)d 0.00(0.14%) f 0.00(0.01%) 23.293% Ti 84 s(13.21%)p 0.01(0.15%)d 6.56(86.62%) f 0.00(0.02%)	Shortened NLMO Analysis of Ti(84)-P(82)Ter π-bond (threshold > 1.3%) 158. (2.00000) 91.5439% BD (2) P 82-Ti 84 47.393% P 82 s(0.29%)p99.99(99.43%)d 0.90(0.26%) f 0.07(0.02%) 1.345% P 83 s(0.08%)p99.99(91.94%)d99.99(7.70%) f 3.60(0.28%) 44.415% Ti 84 s(0.01%)p 1.00(0.02%)d99.99(99.96%) f 0.50(0.01%)

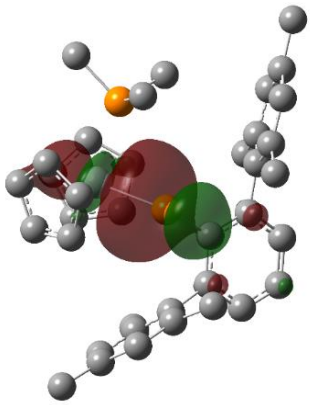	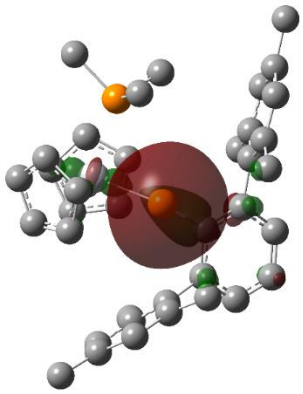 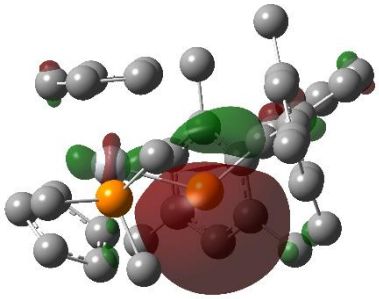
Shortened NLMO Analysis of Ti(84)-P(82)Ter σ-bond (threshold > 1.3%) 157. (2.00000) 94.7179% BD (1) P 82-Ti 84 1.343% C 1 s(3.08%)p31.17(95.91%)d 0.29(0.90%) f 0.04(0.11%) 62.574% P 82 s(24.57%)p 3.05(75.05%)d 0.01(0.35%) f 0.00(0.04%) 32.637% Ti 84 s(8.90%)p 0.01(0.06%)d10.23(91.03%) 0.00(0.01%)	Shortened NLMO Analysis of LP at P(82) (threshold > 1.5%) 59. (2.00000) 90.7432% LP (1) P 82 1.612% C 1 s(6.12%)p15.09(92.32%)d 0.22(1.35%) f0.03(0.21%) 90.811% P 82 s(61.69%)p 0.62(38.26%)d 0.00(0.06%) f 0.00(0.00%) 3.800% Ti 84 s(20.03%)p 0.00(0.02%)d 3.99(79.89%) f 0.00(0.06%)

Table S12. Summary of selected NLMO's of $Cp_2Ti(PMe_3)^{Dip}AsTer$ (**5**).

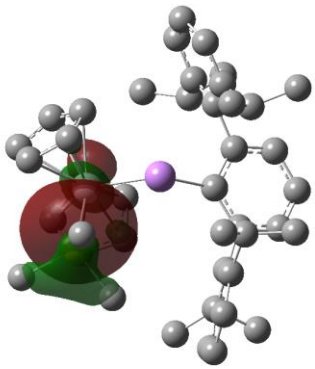	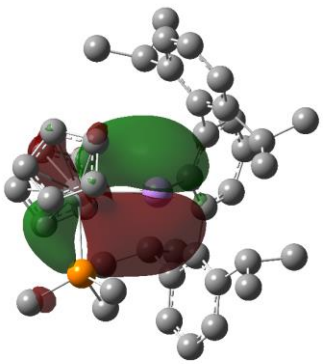

Shortened NLMO Analysis of Ti(1)-P(55)Me_3 σ-bond (threshold > 1.3%) 75. (2.00000) 96.6234% BD (1)Ti 1- P 55 23.800% Ti 1 s(13.04%)p 0.01(0.13%)d 6.66(86.81%) f 0.00(0.02%) 73.231% P 55 s(45.35%)p 1.20(54.51%)d 0.00(0.13%) f 0.00(0.01%)	Shortened NLMO Analysis of Ti(1)-As(102)Ter π-bond (threshold > 1.3%) 44.421% Ti 1 s(0.02%)p 1.29(0.03%)d99.99(99.94%) f 0.51(0.01%) 46.100% As102 s(0.40%)p99.99(99.43%)d 0.41(0.16%) f 0.04(0.02%)
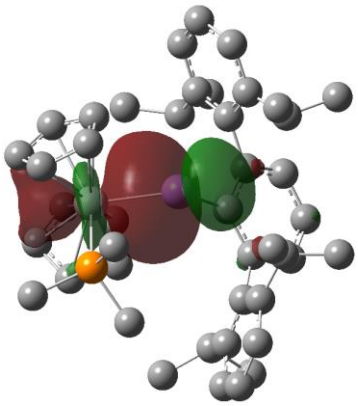	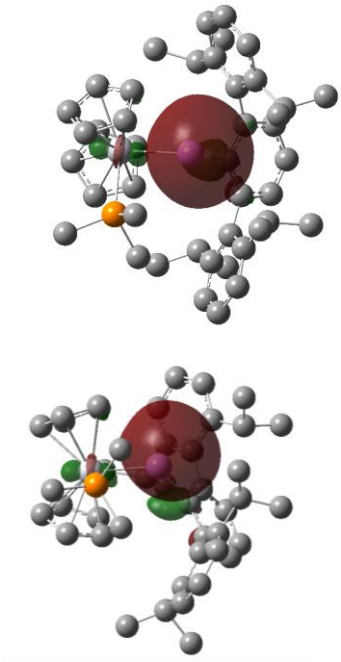
Shortened NLMO Analysis of Ti(1)-As(102)Ter σ-bond (threshold > 1.3%) 76. (2.00000) 94.7659% BD (1)Ti 1-As102 34.287% Ti 1 s(9.19%)p 0.01(0.09%)d 9.88(90.71%) f 0.00(0.02%) 60.877% As102 s(20.37%)p 3.89(79.29%)d 0.01(0.30%) f 0.00(0.03%)	Shortened NLMO Analysis of LP at As(102) (threshold > 1.5%) 74. (2.00000) 93.0616% LP (1)As102 3.123% Ti 1 s(19.71%)p 0.00(0.01%)d 4.07(80.23%) f 0.00(0.06) 93.070% As102 s(68.65%)p 0.46(31.31%)d 0.00(0.03%) f 0.00(0.00%)

5.3.2 QT-AIM analysis of $Cp_2Ti(PMe_3)^{Mes}PTer$ (3) and $Cp_2Ti(PMe_3)As^{Dip}Ter$ (5)

QT-AIM analysis[16] for $Cp_2Ti(PMe_3)P^{Mes}Ter$ (**3**) revealed two Ti–P "bond" paths (Ti(84)–P(82) and Ti(84)–P(82)), in agreement with the Lewis resonance scheme (***Scheme S1***). In addition to the contour plot of the Laplacian of the electron density $\nabla^2 r$ of Ti complex **3** we added the wiberg bond indices (WBI) next to the bond critical points in italic numbers (***Figure S20***). The WBI of 1.73 for the Ti(84)-P(82) bond clearly reveals a double bond on the basis of this theory. The QT-AIM analysis for $Cp_2Ti(PMe_3)As^{Dip}Ter$ can be interpreted in the same manner (***Figure S21***). We found "bond" paths between the titanium center the phosphorus and arsenic atoms. Also in this case the WBI of the Ti(1)-As(102) bond with 1.72 clearly indicates a double bond within the framework of this theory.

Figure S20: Contour plot of the Laplacian of the electron density $\nabla^2 r$ of Ti complex **3** in the P-Ti-P plane. Dashed lines indicate negative (local charge concentration), solid lines indicate positive values (local charge depletion). The Laplacian plot is overlaid with the molecular graph from QT-AIM analysis and wiberg bond indices (italic small numbers). Brown lines indicate bonding paths, blue dots correspond to bond critical points. Density from B3LYP/GD3BJ/def2tzvp calculation.

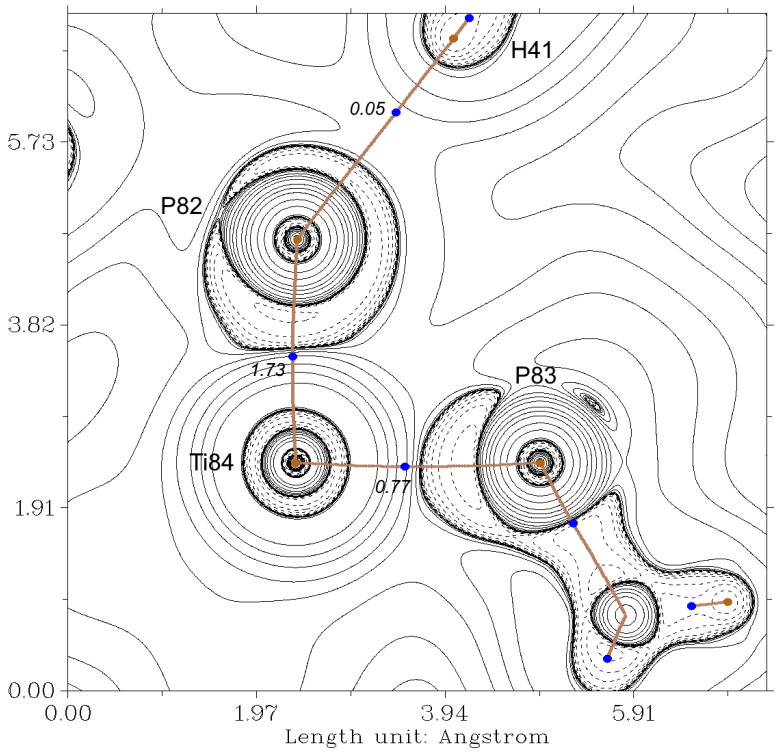

Figure S21: Contour plot of the Laplacian of the electron $\nabla^2 r$ r of Ti complex **5** in the P-Ti-As plane. Dashed lines indicate negative (local charge concentration), solid lines indicate positive values (local charge depletion). The Laplacian plot is overlaid with the molecular graph from QT-AIM analysis and wiberg bond indices (italic small numbers). Brown lines indicate bonding paths, blue dots correspond to bond critical points. Density from B3LYP/GD3BJ/def2tzvp calculation.

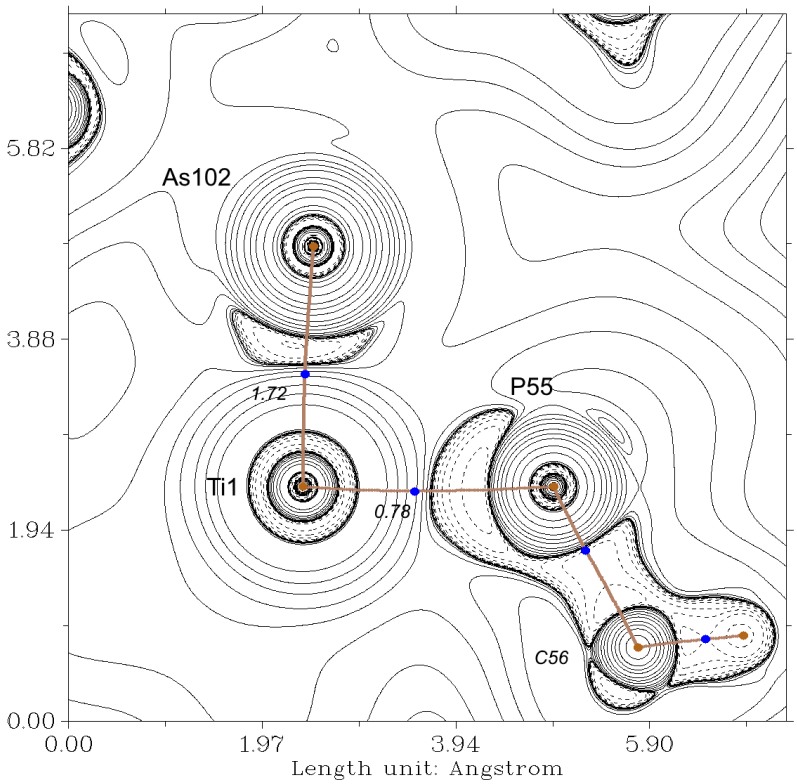

5.3.3 Electron Localisation Function of $Cp_2Ti(PMe_3)^{Mes}PTer$ (3) and $Cp_2Ti(PMe_3)As^{Dip}Ter$ (5)

To further classify the bonding situation in $Cp_2Ti(PMe_3)P^{Mes}Ter$ and $Cp_2Ti(PMe_3)As^{Dip}Ter$ we had a closer look to the 3D-plots of the electron localization functions (ELF). The results from QT-AIM- and NBO-analysis are corroborated by ELF analysis (***Figure S22*** and ***Figure S23***) showing a dative Ti(84)-P(83)Me_3 bond and a lone pair at the P(82) atom. Furthermore, there is a dumbbell-shaped ELF between the titanium center and the phosphinidene phosphorus atom which indicates a Ti=P double bond based on this theory. The 3D plot of the ELF for $Cp_2Ti(PMe_3)$AsDipTer can be described in the same manner. We find a dative Ti1-P55 bond as well as a lone pair on As102 and a dumbbell-shaped ELF between Ti(1)-As(102).

Figure S22: 3D-ELF plot of the central $Ti(PMe_3)PAr$ unit in $Cp_2Ti(PMe_3)P^{Mes}Ter$ (**3**).

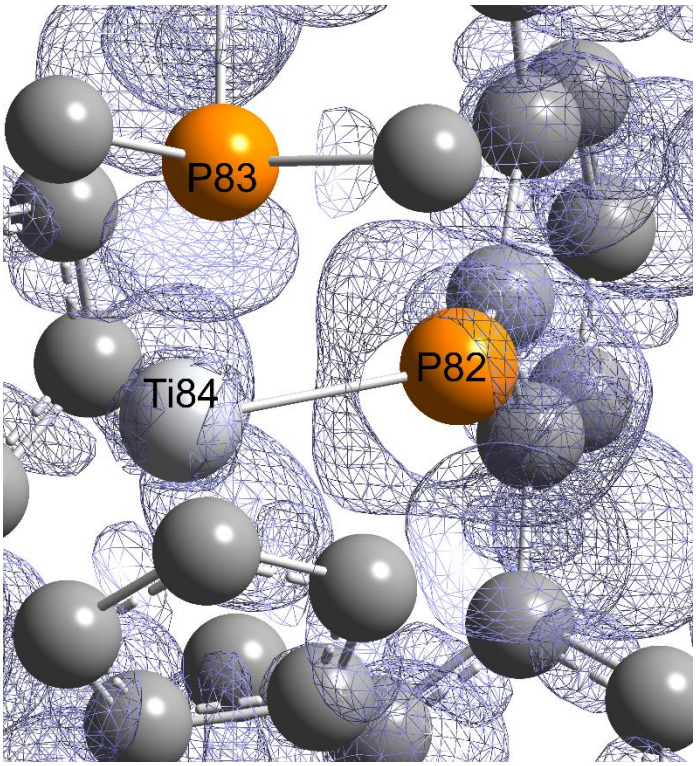

Figure S23: 3D-ELF plot of the central $Ti(PMe_3)AsAr$ unit in $Cp_2Ti(PMe_3)As^{Dip}Ter$ (**5**).

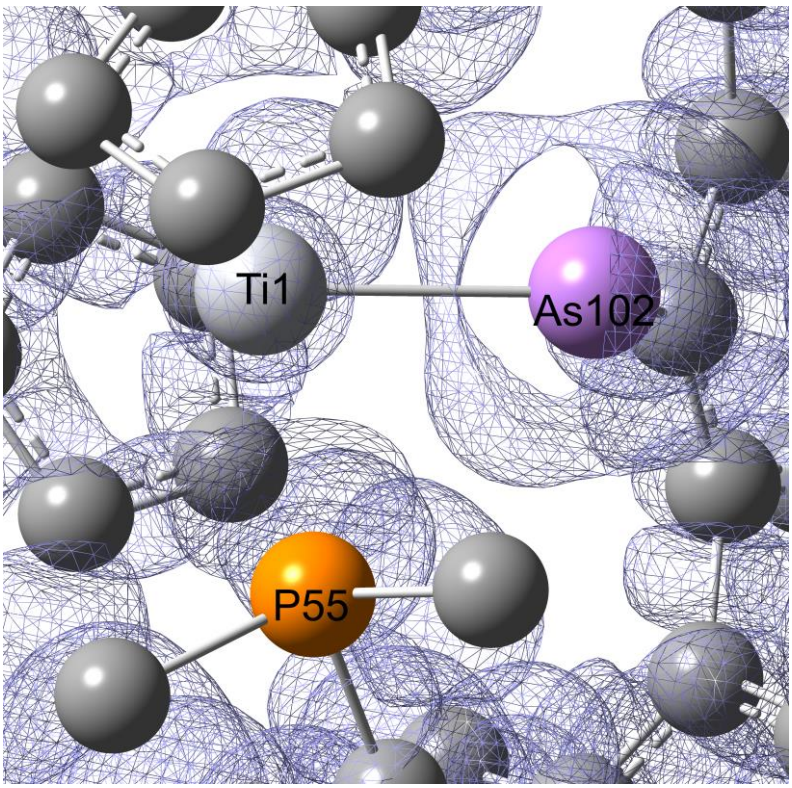

5.3.4 Proof of the wavefunction stability of $Cp_2Ti(PMe_3)P^{Mes}Ter$ (3), $Cp_2Ti(PMe_3)As^{Dip}Ter$ (5) and comparable literature complexes II-V

In order to proof the correctness of the electronical description of the complexes **3** and **5** described here and selected literature compounds **II**-**V**, we first proofed the stability of the Kohn-Sham wavefunctions of the performed DFT calculations (B3LYP/GD3BJ/def2svpp of def2tzvp). We found in all investigated systems stable closed shell KS wavefunctions. To take the results from the NBO calculations into account, which gives indication of a potentially open shell singlet state (biradicaloid character), we next proofed the stability of the Hatree-Fock (HF) wavefunctions. To our surprise we find in all cases an RHF/UHF instability of these. With a closer look to the spin density of these optimised UHF calculations we notice in all cases opposing spin densities located at the metal center and the pnictogen atoms (***Table S13***). Moreover, we obtain high spin contaminations of the aromatic ligand systems. Nevertheless, these results are an indicator for considering those molecules as biradicaloid's, or in other words, bearing an antiferromagnetic coupled electron pair as π-bond system. Therefore, we performed simple Complete Active Space (CAS) calculations considering just two electrons in two orbitals (see next section). We choose the orbitals which are in line with the examined spin density plots as active space.

Table S13. Representation of the spindensity plots of the investigated compounds at isovalue 0.01.

Compound **3**	Compound **5**

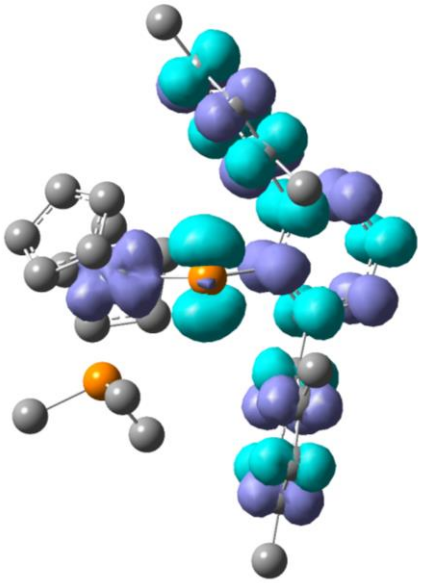	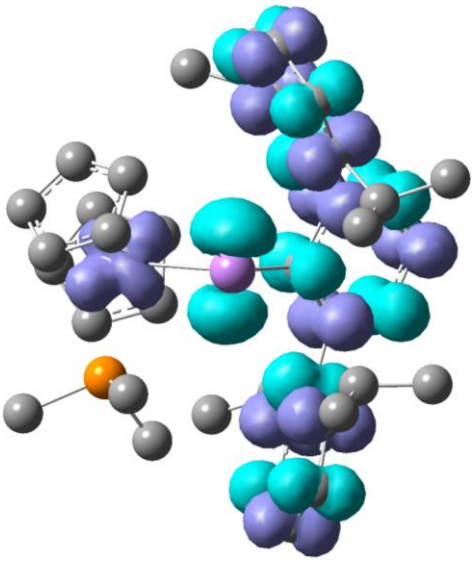
Complex **II**	Complex **III**
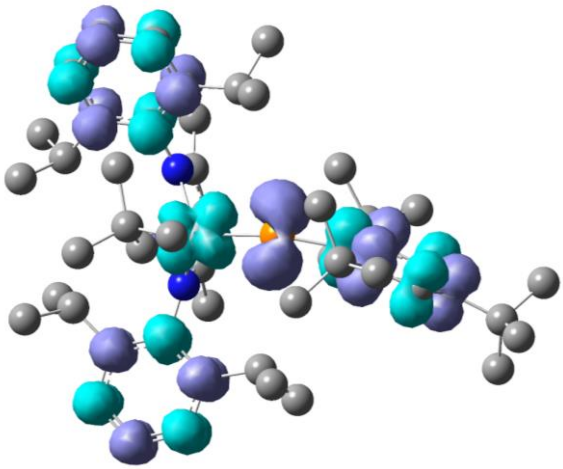	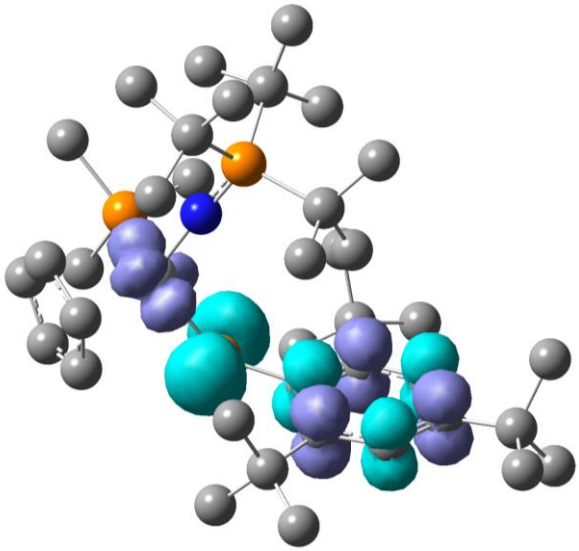
Complex **IV**	Complex **V**

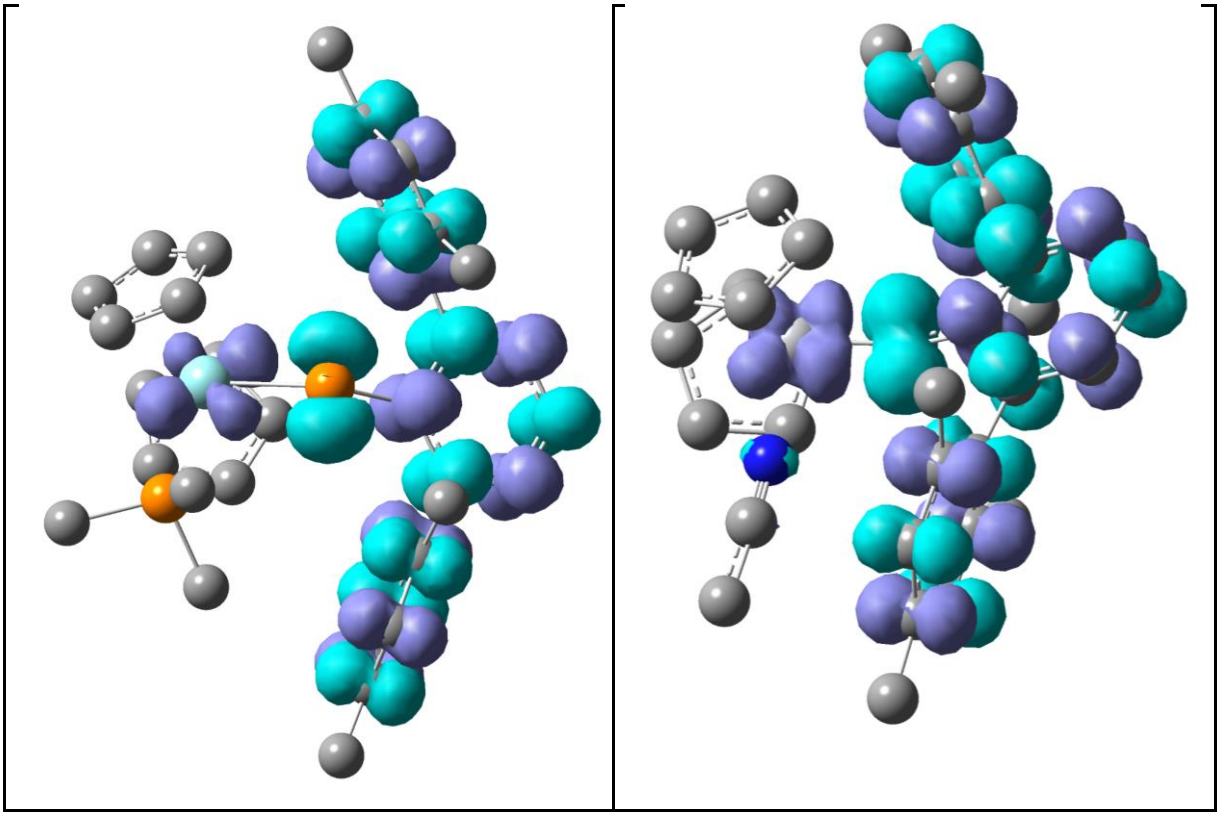

5.3.5 Biradical character of $Cp_2Ti(PMe_3)P^{Mes}Ter$ (3) and $Cp_2Ti(PMe_3)As^{Dip}Ter$ (5)

The "broken-symmetry" solution is not a true eigenfunction of the S^2 operator. In fact, it may be considered as a 50:50 mixture of the singlet and triplet state, if the overlap between the singly occupied orbitals and spin polarisation are small.[17] The actual singlet wave function can then be expressed in terms of a linear combination of *two* "broken-symmetry" wave functions

$$^1\Psi = \frac{1}{\sqrt{2}}\left(|\cdots \chi_+\overline{\chi_-}\rangle - |\cdots \overline{\chi_+}\chi_-\rangle\right)$$

where χ_+, χ_- are the singly occupied orbitals and the overline indicates β spin. Therefore, the open-shell singlet must be described by a multi-reference wave function.

In the "broken-symmetry" picture, the singly occupied orbitals χ_+ and χ_- are, in principle, localised orbitals formed by linear combinations of the (delocalised) canonical HOMO ϕ_{H} and LUMO ϕ_{L}:

$$\chi_{\pm} = \frac{1}{\sqrt{2}}(\phi_H \pm \phi_{\mathrm{L}})$$

Hence, the multi-reference wave function expressed in terms of the canonical MOs is given by

$$^{1}\Psi = c_1|\cdots\phi_{\mathrm{H}}^2\rangle + c_2|\cdots\phi_{\mathrm{L}}^2\rangle$$

where the expansion coefficients c_i are the square roots of the relative weight of each determinant. This type of multi-determinant open-shell singlet wave function can be obtained by the Complete Active Space (CAS) SCF method and gives a qualitatively correct description of the electronic structure of a biradical. The biradical character can be evaluated as

$$\beta = \frac{2c_2^2}{c_1^2 + c_2^2}$$

where a value of β = 1 indicates a "perfect" biradical with two electrons in two degenerate orbitals.[18] Smaller values indicate an increasing energy gap between HOMO and LUMO, and $\beta \rightarrow 0$ indicates a closed-shell species.

Consequently, the smallest active space to properly describe a biradical is a CAS(2,2) calculation (*i.e.* two electrons in two orbitals). In case of compounds **3** and **5**, this calculation show that the contributions to the multi-determinant wave function are the two determinants placing two electrons either in the formal HOMO (ϕ_1) or LUMO (ϕ_2) lead to a biradical character of β = 37 % for $Cp_2Ti(PMe_3)^{Mes}PTer$ (**3**) and 40 % for $Cp_2Ti(PMe_3)As^{Dip}Ter$ (**5**).

Figure S24: Schematic depiction of the active orbitals of a CAS(2,2) calculation (def2svpp) of the $Cp_2Ti(PMe_3)P^{Mes}Ter$ (**3**). The orbital localization scheme indicates that one of the radical centers is localized at Ti, while the other is localized at the phosphinidene phosphorus atom.

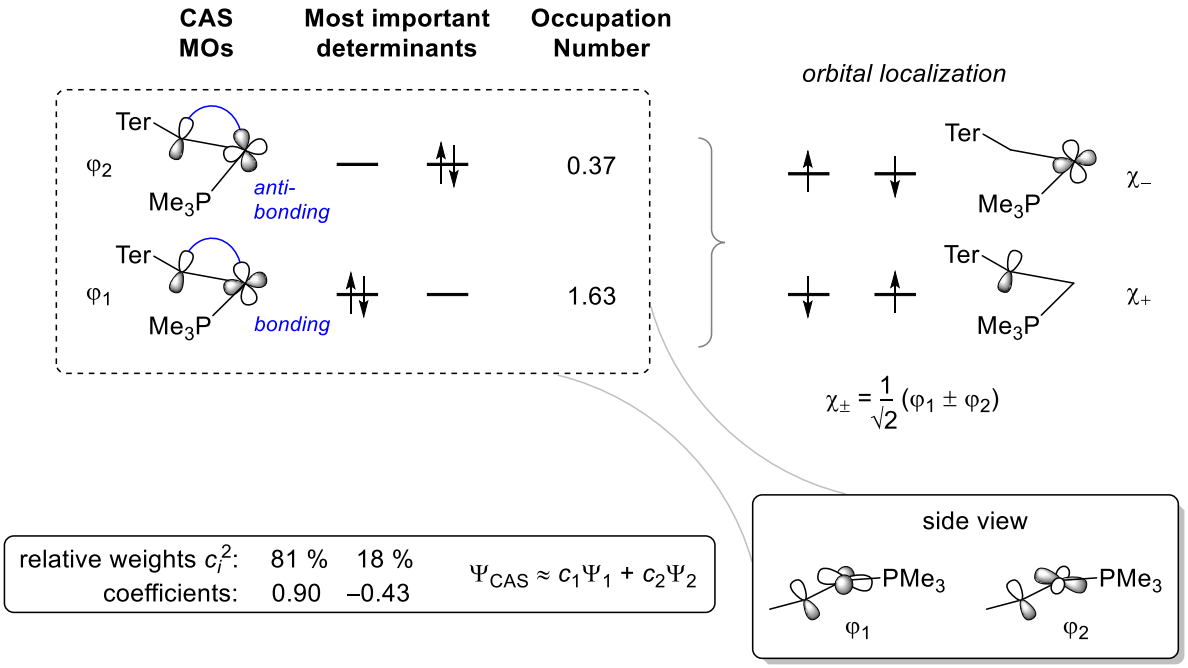

Figure S25: Schematic depiction of the active orbitals of a CAS(2,2) calculation (def2svpp) of the $Cp_2Ti(PMe_3)As^{Dip}Ter$ (**5**). The orbital localisation scheme indicates that one of the radical centres is localised at Ti, while the other is localised at the phosphinidene phosphorus atom.

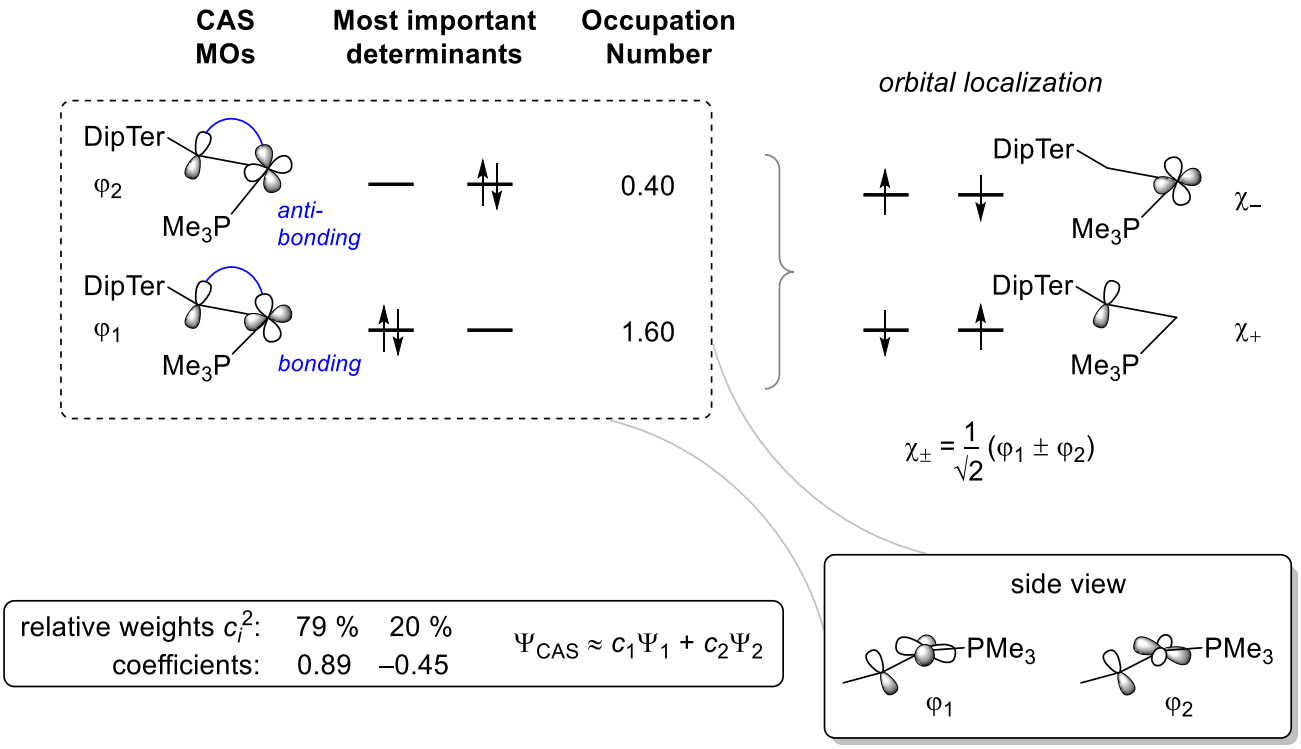

Hence, compounds **3** and **5** can be regarded as a biradicals. The singlet states are calculated to be the ground states ($\Delta E_{S\text{-}T}$ = −106.2 kJ/mol for **3** and −96.6 kJ/mol for **5**); i.e. the radical centres are strongly antiferromagnetically coupled. The calculated exchange coupling constants[19] are.

$$2J(\mathbf{3}) = E_{\mathrm{S}} - E_{\mathrm{T}} = -8881.2\ \mathrm{cm}^{-1}$$

$$2J(\mathbf{5}) = E_{\mathrm{S}} - E_{\mathrm{T}} = -8075.9\ \mathrm{cm}^{-1}$$

The radical centers are localized at Ti and on the phosphorus atom of the phosphinidene or arsenic atom of the arsinidene ligand (***Figure S24*** and ***Figure S25***), respectively. Therefore, the electronic structure can be understood as a complex between a formal Ti(III) fragment and a phosphorus or arsenic centered radical, whose "free" electrons are antiferromagnetically coupled. Therefore, complexes **3** and **5** are EPR-silent in their respective ground states. To proof the general description of group 4 pnictinidenes as biradicoloids we further performed the same calculations for the literature known complexes (**II-V**). Through the calculations of complex **II** and **V** we noticed two sets of formally Ti-E (E = P, N) π-bonds consisting of orthogonal d-shaped orbitals at titanium and p-shaped orbitals at the pnictogen atom. This was described in the original literature resulting in a pseudo Ti-P triple bond.[20] To take this into account we increased, in these complexes, the active space considering four electrons in four molecular orbitals (CAS(4,4)). This revealed in the complexes **II** and **V** the expected biradical character alongside a small degree of formally tetra radical character. It should be noted that the smaller CAS(2,2) calculations intrinsically lead to larger β values compared to larger active space calculations and may overestimate this value as they do not account for dynamic correlations. Nevertheless, we have summarized in ***Table S14*** the calculated occupation numbers of the orbitals considered. In the case of the CAS(2,2) calculations, these values of the ϕ_{L} are mathematically identical with the beta value.

Table S14. Summary of all calculated biradical character β from CAS(2,2)/def2svpp calculations and $\Delta E_{S\text{-}T}$ (B3LYP/GD3BJ/def2tzvp).

Compound	**Occupation numbers**	**Singlet Triplet gap $\Delta E_{S\text{-}T}$**
$Cp_2Ti(PMe_3)P^{Mes}Ter$ (**3**)	$\phi_1 = 1.63$ $\phi_2 = 0.37$	−106.2 kJ/mol
$Cp_2Ti(PMe_3)As^{Dip}Ter$ (**5**)	$\phi_1 = 1.60$ $\phi_2 = 0.40$	−96.6 kJ/mol
Complex **II**	$\phi_1 = 1.88$ $\phi_2 = 1.85$ $\phi_3 = 0.15$ $\phi_4 = 0.12$	−122.92 kJ/mol[a]
Complex **III**	$\phi_1 = 1.67$ $\phi_2 = 0.33$	−121.22 kJ/mol
Complex **IV**	$\phi_1 = 1.84$ $\phi_2 = 0.16$	−149.81 kJ/mol
Complex **V**	$\phi_1 = 1.93$ $\phi_2 = 1.86$ $\phi_3 = 0.14$ $\phi_4 = 0.07$	−214.90 kJ/mol

[a] In case of this complex the def2tzvp calculation did not converged, therefore we calculated this value on the basis of single point def2svpp calculations considering the optimised structure of the higher basis.

Table S15. Representation of the ϕ_1 and ϕ_2 of the CAS(2,2) calculations.

Compound **3** $\boldsymbol{\phi_1}$	Compound **3** $\boldsymbol{\phi_2}$
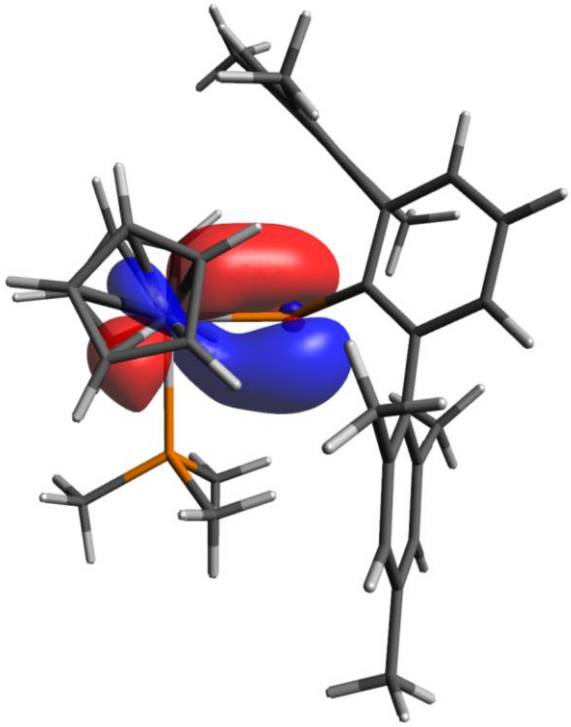	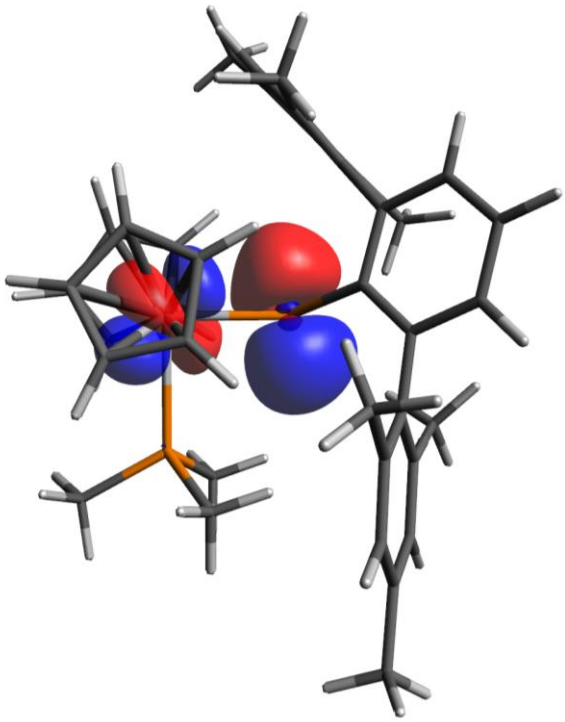
Compound **5** $\boldsymbol{\phi_1}$	Compound **5** $\boldsymbol{\phi_2}$
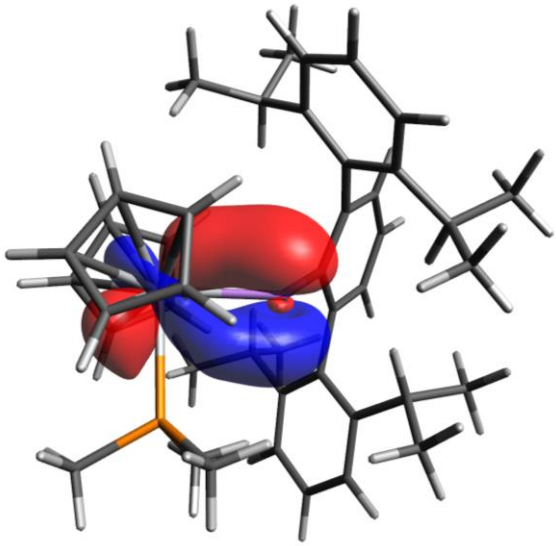	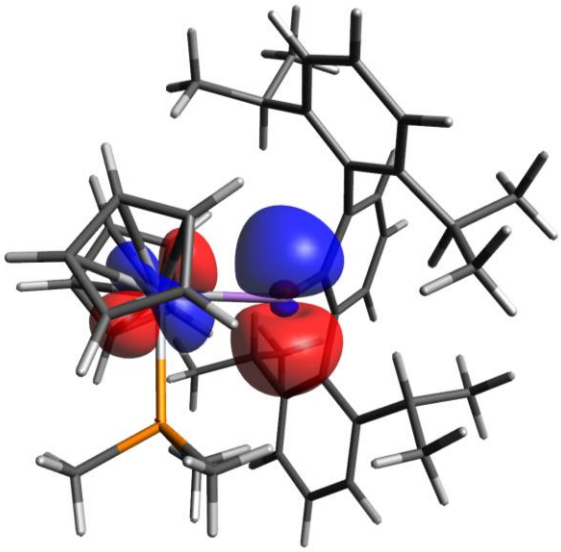
Compound **II** $\boldsymbol{\phi_1}$	Compound **II** $\boldsymbol{\phi_2}$

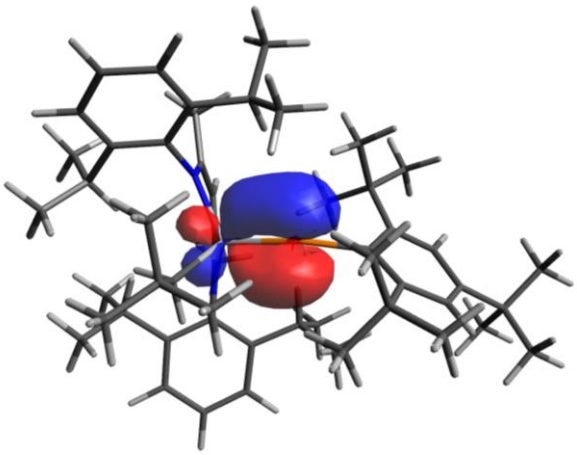

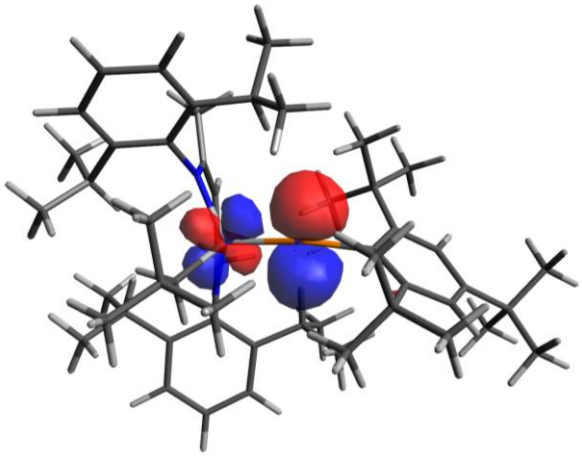

Compound **III** $\boldsymbol{\phi_1}$

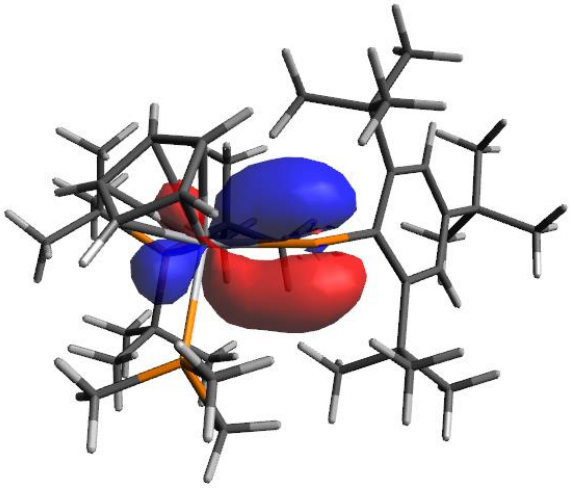

Compound **III** $\boldsymbol{\phi_2}$

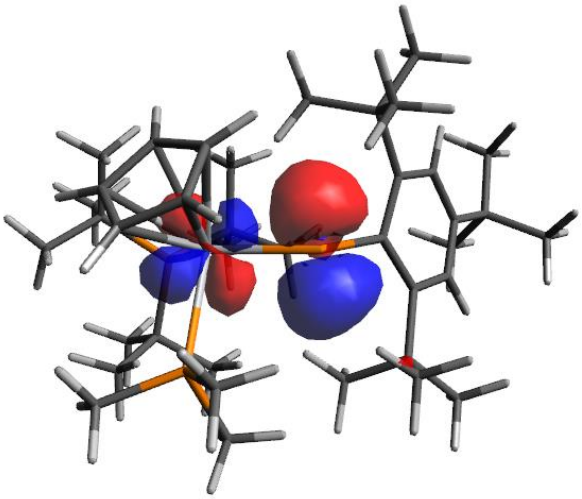

Compound **IV** $\boldsymbol{\phi_1}$

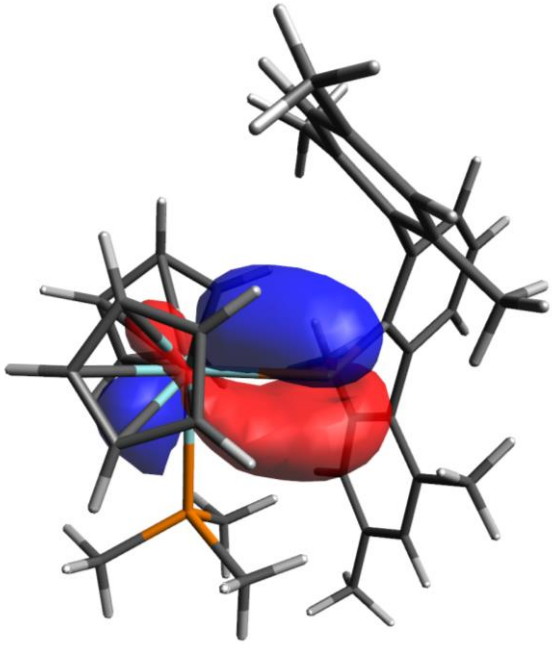

Compound **IV** $\boldsymbol{\phi_2}$

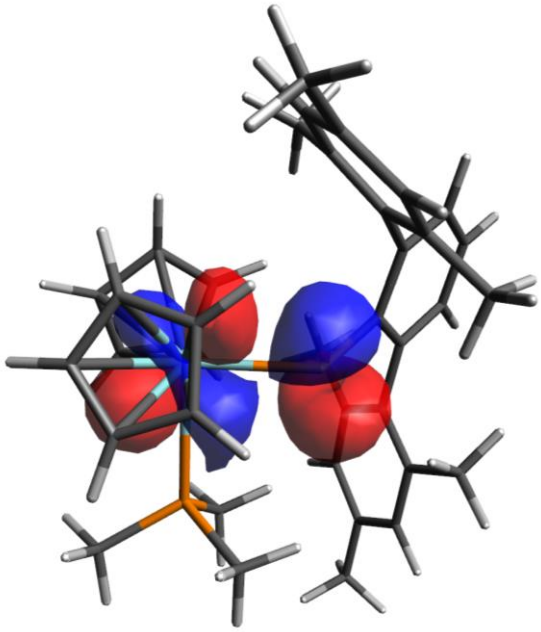

Compound **V** $\boldsymbol{\phi_1}$	Compound **V** $\boldsymbol{\phi_2}$
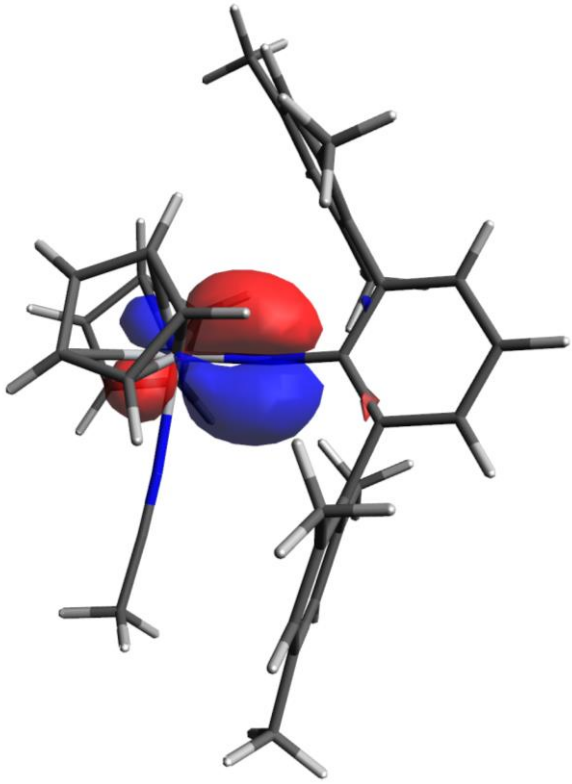	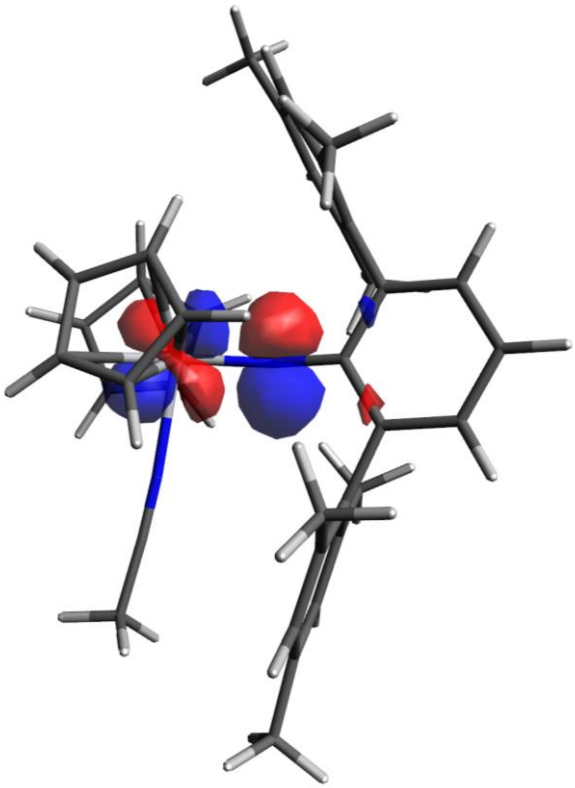

5.3.6 Calculation of the theoretical ^{31}P NMR chemical shifts of the phosphorus atoms in $Cp_2Ti(PMe_3)P^{Mes}Ter$ and $Cp_2Ti(PMe_3)As^{Dip}Ter$

Chemical shifts were derived by the GIAO method at the PBE0/def2svp level of theory using the optimized structures from B3LYP/GD3BJ/def2tzvp calculations.[21] The calculated absolute shifts ($\sigma_{calc,X}$) were referenced to the experimental absolute shift of 85% H_3PO_4 in the gas phase ($\sigma_{ref,1}$ = 328.35 ppm),[22] using PH_3 ($\sigma_{ref,2}$ = 594.45 ppm) as a secondary standard:[23]

$$\delta_{calc,X} = (\sigma_{ref,1} - \sigma_{ref,2}) - (\sigma_{calc,X} - \sigma_{calc,PH_3})$$
$$= \sigma_{calc,PH_3} - \sigma_{calc,X} - 266.1 \text{ ppm}$$

At the PBE0/def2-SVP level of theory, σ_{calc,PH_3} amounts to +629.20 ppm. With these data in hand we were able to calculate the ^{31}P NMR chemical shifts of the complexes **3** and **5**, which are in reasonable agreement with the experimental values.

Table S16. Summary of all calculated ^{31}P NMR shifts.

Compound	**Ti-*PR*$_3$**	**Ti-*P*R**
$Cp_2Ti(PMe_3)P^{Mes}Ter$ (**3**)	404.29 → -41.19 ppm	-799.08 → 1162.12 ppm
$Cp_2Ti(PMe_3)As^{Dip}Ter$ (**5**)	402.12 → -39.02 ppm	-
Complex **II**	-	121,76 → 241.34 ppm
Complex **III**	370.47/420.05 → -7.37/-56.95 ppm	-280.50 → 643.60 ppm
Complex **IV**	415.49 → -52.39 ppm	-407.41 → 770.51 ppm

5.3.7 Comparison of the experimental and calculated UV/Vis spectra of $Cp_2Ti(PMe_3)P^{Mes}Ter$ and $Cp_2Ti(PMe_3)As^{Dip}Ter$

These calculations were performed to gain a deeper understanding about the colour of the herein described complexes. The calculations were performed on the former described B3LYP/GD3BJ/def2tzvp level of theory considering 40 excited states as well as the scrf approach for THF as solvent. The calculated data were plotted with a half-width of 2000 cm^{-1} and normalized to a prominent band of the experimentally

observed spectrum. For the experimental measurement of the UV/Vis spectra of both complexes we diluted approximately 1 mg of complex in 4 mL THF under Ar-atmosphere. Due to the large UV absorption of the terphenyl substituents the spectrum was not well resolved, especially in the UV region, and we diluted the Sample approx. 1:4 (we note that upon dilution a partial decomposition of **3** cannot be ruled out, which might explain the deviation of the calculated and the experimental spectra). Those prepared samples of the compound **3** showed only small shoulders next to the strong UV band in the Vis region from which the λ_{max} values are difficult to specify. In contrast to this the spectrum of **5** shows two broad absorption maxima at λ = 652 and 474,5 nm in the Vis region and one further prominent band at λ = 353,5 nm which tailed out in the Vis region. These experiments are well in line with the observations by our naked eyes were the color of compound **5** is much more intense compared to complex **3**. As expected, revealed the calculations a more complex excitation behavior for both complexes. The first excitation states (λ_{EX1}(**3**) = 634 nm; λ_{EX1}(**5**) = 652 nm) can be explained by an excitation by electrons from the highest occupied molecular orbital (HOMO) as well as the HOMO-1 into the lowest unoccupied molecular orbital (LUMO) (***Table S17*** and ***Table S18***). These both donor molecular orbitals can be best described as titanium – phosphorus/arsenic binding molecular orbitals which together form the Ti=P/As double bond. This is in line with the shape of the acceptor LUMO which can be described as Ti-P/As antibonding molecular orbital. The following 17 excited states, which also possess the HOMO and HOMO-1 as donor molecular orbitals, combine transitions of various LUMO orbitals that can be described mainly as antibonding molecular orbitals of the terphenyl substituents.

Figure S26: Plot of the UV/Vis spectra and the calculated oscillator strength of $Cp_2Ti(PMe_3)P^{Mes}Ter$ (**3**).

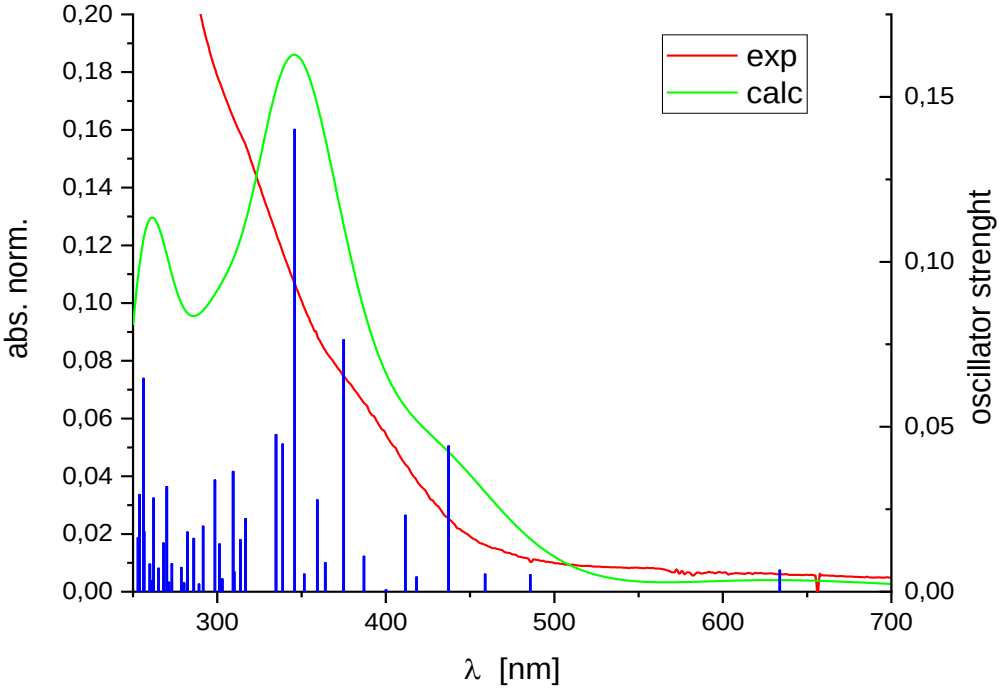

Figure S27: Plot of the UV/Vis spectra and the calculated oscillator strength of $Cp_2Ti(PMe_3)As^{Dip}Ter$ (**5**).

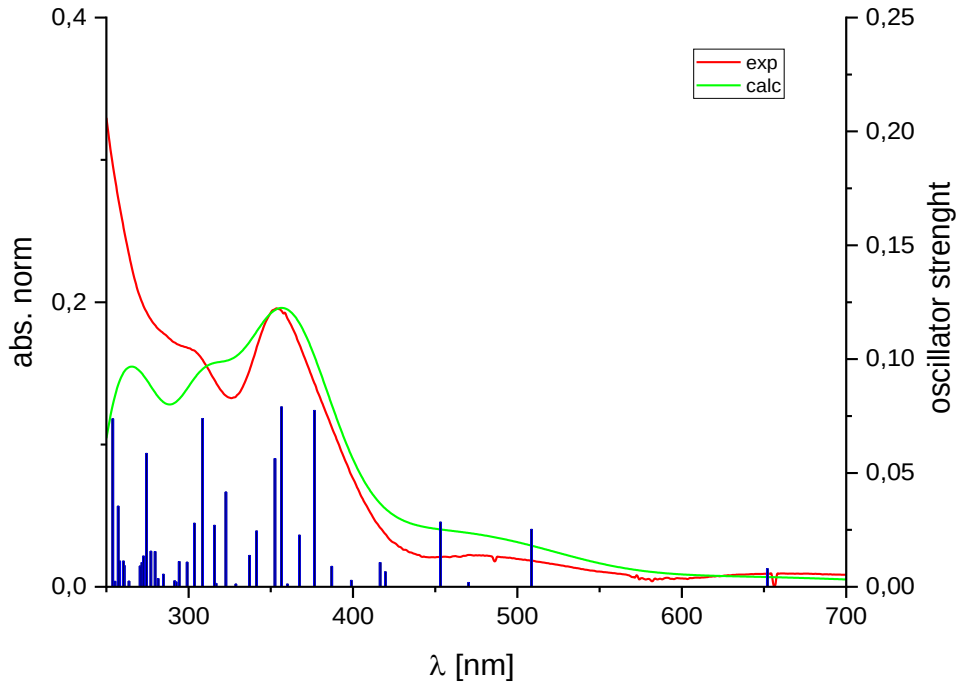

5.3.7.1 Report of the first 20 excited states of $Cp_2Ti(PMe_3)P^{Mes}Ter$ (3) and corresponding molecular orbitals

```
Cp2Ti_PTer_PMe_UV_old_THFsolv
---------------------------------------------------------------------
# b3lyp empiricaldispersion=gd3bjdef2tzvp geom=allcheck guess=read TD
=(Nstates=20) scrf=(pcm,solvent=THF)
---------------------------------------------------------------------

Excitation energies and oscillator strengths:

Excited State  1:      Singlet-A     1.9563 eV  633.77 nm  f=0.0065  <S**2>=0.000
    158 -> 160        0.27486
    159 -> 160        0.64251
This state for optimization and/or second-order correction.
Total Energy, E(TD-HF/TD-DFT) =  -2969.46321641
Copying the excited state density for this state as the 1-particle RhoCI density.

Excited State  2:      Singlet-A     2.5526 eV  485.72 nm  f=0.0052  <S**2>=0.000
    158 -> 160        0.46997
    158 -> 162        0.15559
    159 -> 160       -0.16282
    159 -> 161       -0.24648
    159 -> 162       -0.27666
    159 -> 163        0.16983
    159 -> 164        0.17881

Excited State  3:      Singlet-A     2.7017 eV  458.92 nm  f=0.0054  <S**2>=0.000
    158 -> 160        0.16145
    158 -> 162       -0.14499
    159 -> 161       -0.22928
    159 -> 162        0.57789
    159 -> 164        0.19168

Excited State  4:      Singlet-A     2.8356 eV  437.23 nm  f=0.0442  <S**2>=0.000
    158 -> 160        0.29699
    158 -> 161       -0.24843
    158 -> 162        0.16261
    158 -> 164        0.17390
    159 -> 160       -0.12793
    159 -> 161        0.37792
    159 -> 162        0.13553
    159 -> 163       -0.16545
    159 -> 164       -0.21946

Excited State  5:      Singlet-A     2.9642 eV  418.28 nm  f=0.0045  <S**2>=0.000
    158 -> 162       -0.31886
    158 -> 163        0.12665
    158 -> 166       -0.18250
    159 -> 162       -0.14923
    159 -> 164        0.11282
    159 -> 165       -0.12407
    159 -> 166        0.46652
    159 -> 167        0.14048
    159 -> 168        0.16460

Excited State  6:      Singlet-A     3.0123 eV  411.59 nm  f=0.0231  <S**2>=0.000
    158 -> 162        0.12623
    158 -> 164       -0.15408
    159 -> 161        0.36942
    159 -> 163        0.12085
    159 -> 164        0.46793
    159 -> 167        0.18158
    159 -> 168       -0.11712
    159 -> 171       -0.10553

Excited State  7:      Singlet-A     3.0990 eV  400.07 nm  f=0.0006  <S**2>=0.000
```

```
   158 -> 161       0.27164
   158 -> 162       0.41148
   158 -> 163      -0.16400
   158 -> 164      -0.16635
   158 -> 166      -0.18617
   158 -> 168      -0.15422
   159 -> 162       0.11071
   159 -> 163      -0.13145
   159 -> 166       0.26195

Excited State  8:      Singlet-A      3.2034 eV  387.04 nm  f=0.0108  <S**2>=0.000
   158 -> 161       0.12026
   159 -> 161       0.17677
   159 -> 162       0.13803
   159 -> 163       0.58890
   159 -> 164      -0.20185
   159 -> 165      -0.13084

Excited State  9:      Singlet-A      3.3068 eV  374.94 nm  f=0.0764  <S**2>=0.000
   158 -> 160      -0.12535
   158 -> 161      -0.19991
   158 -> 162       0.27656
   158 -> 164       0.36995
   158 -> 166       0.12715
   158 -> 167       0.15916
   159 -> 161      -0.17638
   159 -> 163       0.20701
   159 -> 166       0.21719
   159 -> 167       0.11816

Excited State 10:      Singlet-A      3.4053 eV  364.09 nm  f=0.0088  <S**2>=0.000
   158 -> 161       0.11116
   158 -> 163      -0.15365
   158 -> 164      -0.10443
   158 -> 165      -0.16096
   158 -> 166       0.50576
   158 -> 168       0.21084
   159 -> 165      -0.17275
   159 -> 166       0.19879
   159 -> 168       0.12720

Excited State 11:      Singlet-A      3.4500 eV  359.37 nm  f=0.0279  <S**2>=0.000
   158 -> 161       0.23049
   158 -> 164       0.34748
   158 -> 165       0.10103
   158 -> 167       0.15075
   158 -> 168      -0.10475
   158 -> 171      -0.10298
   159 -> 161       0.15772
   159 -> 164       0.26494
   159 -> 165      -0.17541
   159 -> 166      -0.12541
   159 -> 167      -0.26805
   159 -> 168       0.15763

Excited State 12:      Singlet-A      3.5261 eV  351.61 nm  f=0.0054  <S**2>=0.000
   159 -> 165       0.53012
   159 -> 166       0.24066
   159 -> 167      -0.37938

Excited State 13:      Singlet-A      3.5849 eV  345.85 nm  f=0.1401  <S**2>=0.000
   158 -> 161       0.39842
   158 -> 164       0.19611
   159 -> 164      -0.10429
   159 -> 165       0.27783
   159 -> 167       0.39156

Excited State 14:      Singlet-A      3.6593 eV  338.82 nm  f=0.0448  <S**2>=0.000
   158 -> 161      -0.22968
   158 -> 163      -0.39894
```

```
   159 -> 165      0.12938
   159 -> 166     -0.14649
   159 -> 167      0.15117
   159 -> 168      0.43860

Excited State 15:      Singlet-A      3.7028 eV  334.84 nm  f=0.0477  <S**2>=0.000
   158 -> 162      0.16808
   158 -> 163      0.48763
   158 -> 164     -0.20105
   159 -> 166     -0.11076
   159 -> 168      0.37451

Excited State 16:      Singlet-A      3.9135 eV  316.81 nm  f=0.0221  <S**2>=0.000
   158 -> 164      0.12576
   158 -> 165     -0.25832
   158 -> 166     -0.14556
   158 -> 167     -0.17546
   158 -> 168      0.18522
   159 -> 167     -0.11615
   159 -> 168      0.12166
   159 -> 169      0.39672
   159 -> 170      0.27461
   159 -> 171     -0.15848

Excited State 17:      Singlet-A      3.9519 eV  313.73 nm  f=0.0159  <S**2>=0.000
   158 -> 165      0.30573
   158 -> 166      0.15708
   158 -> 168     -0.12911
   159 -> 169      0.55034

Excited State 18:      Singlet-A      3.9988 eV  310.05 nm  f=0.0061  <S**2>=0.000
   154 -> 160      0.22555
   156 -> 160     -0.12730
   157 -> 160     -0.11742
   158 -> 165      0.43631
   158 -> 166      0.15026
   158 -> 167     -0.36207
   159 -> 170      0.12930

Excited State 19:      Singlet-A      4.0069 eV  309.43 nm  f=0.0365  <S**2>=0.000
   152 -> 160     -0.11100
   153 -> 160     -0.11411
   154 -> 160      0.42170
   156 -> 160     -0.23659
   157 -> 160     -0.23623
   158 -> 165     -0.19236
   159 -> 169      0.13187
   159 -> 170     -0.25159
   159 -> 171      0.12723

Excited State 20:      Singlet-A      4.0928 eV  302.93 nm  f=0.0039  <S**2>=0.000
   152 -> 160      0.11420
   157 -> 160      0.14644
   158 -> 165      0.19263
   158 -> 166     -0.21365
   158 -> 167      0.15235
   158 -> 168      0.52458
   159 -> 170     -0.19987
   159 -> 171      0.12562
```

Table S17. Representation of the most important molecular orbitals of **3**.

LUMO+7 (167)	LUMO+6 (166)

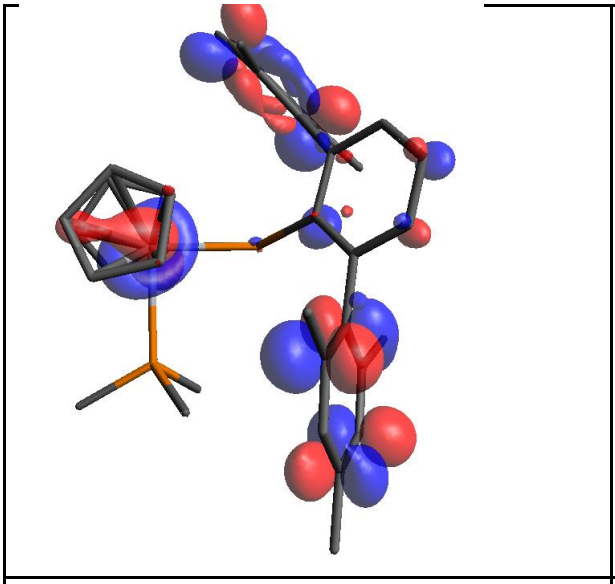	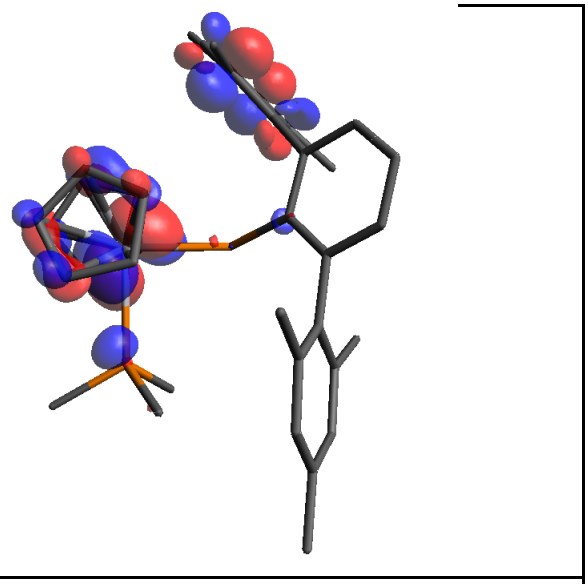
LUMO+5 (165)	LUMO+4 (164)
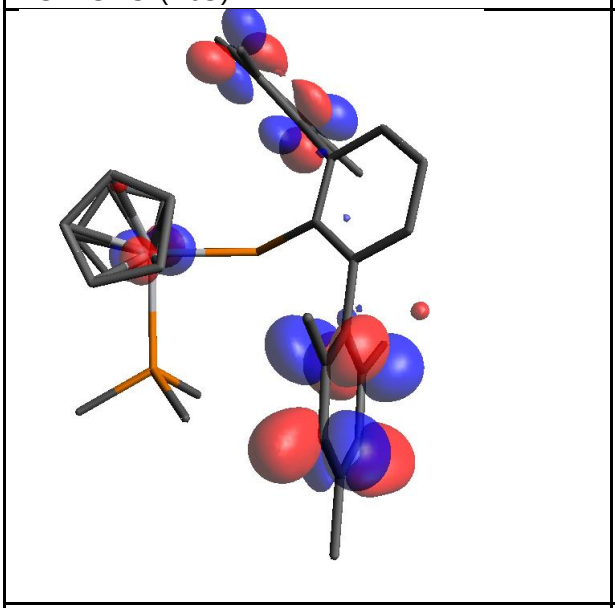	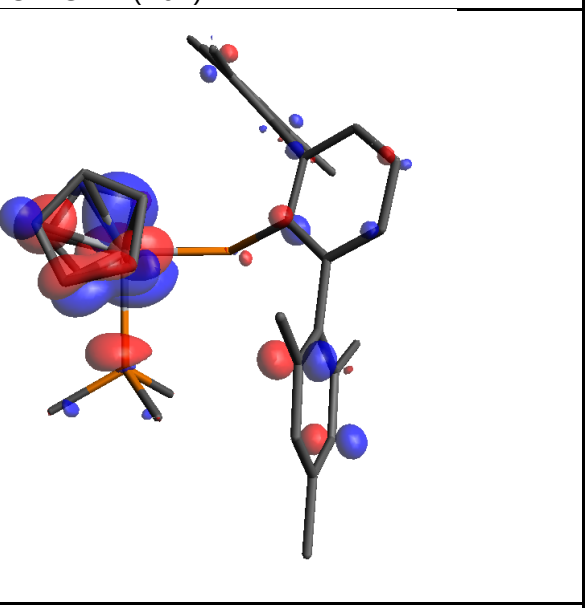
LUMO+3 (163)	LUMO+2 (162)
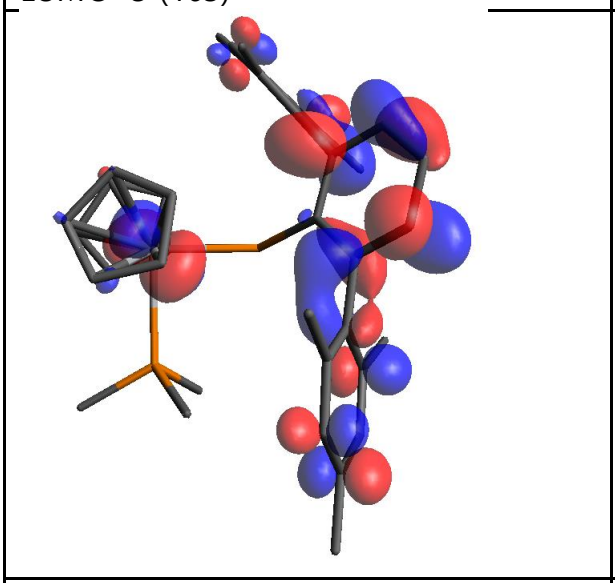	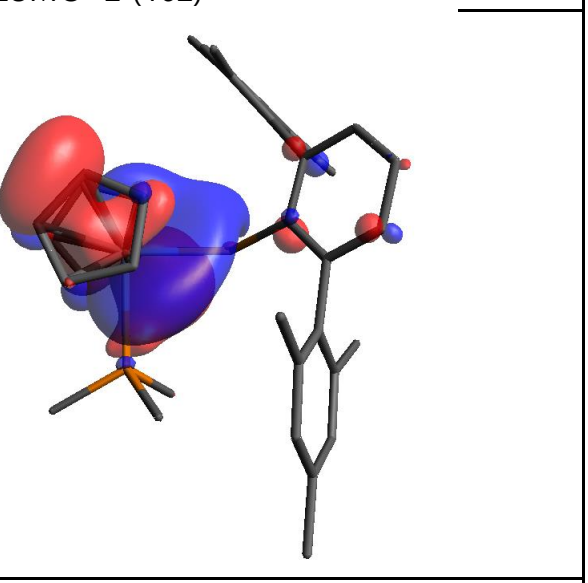
LUMO+1 (161)	LUMO (160)

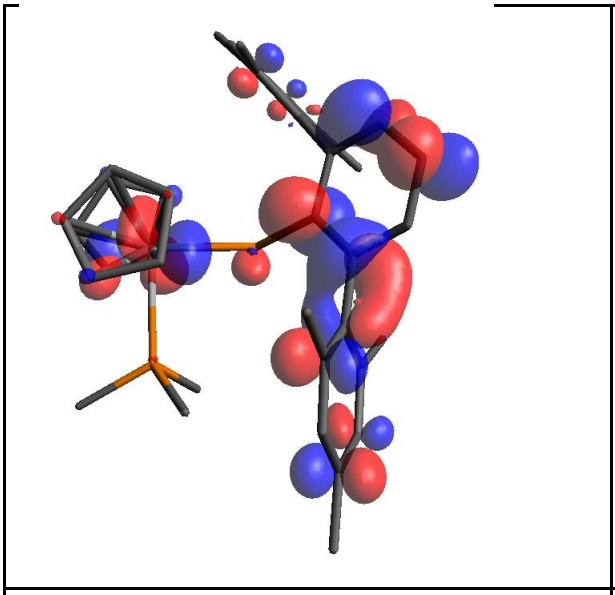

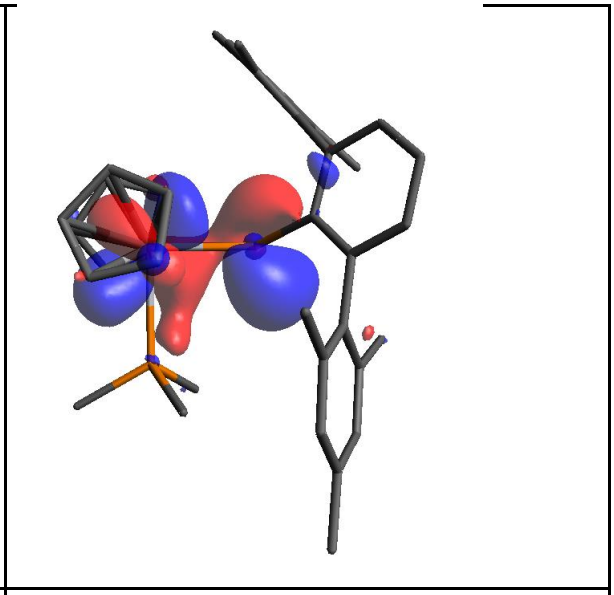

HOMO (159)

HOMO-1 (158)

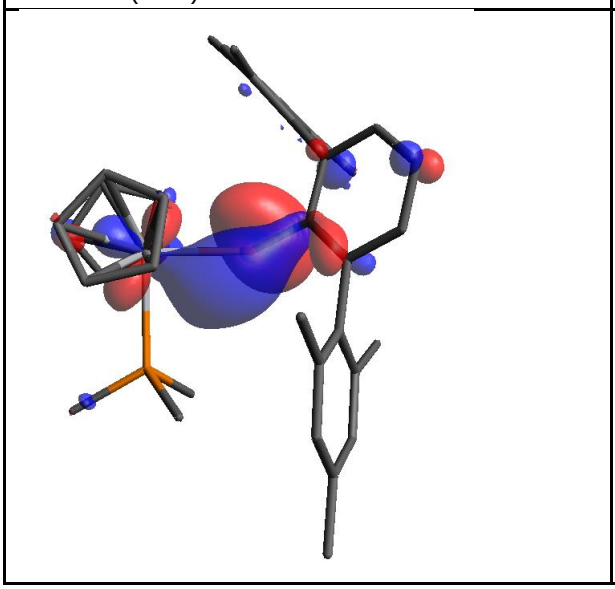

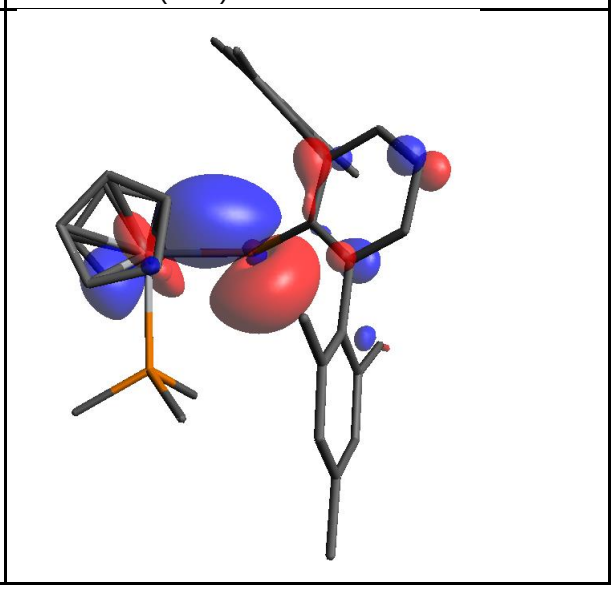

5.3.7.2 Report of the first 20 excited states of $Cp_2Ti(PMe_3)As^{Dip}Ter$ (5) and the corresponding molecular orbitals

```
Cp2Ti_AsDipTer_PMe3__UV_old_THFsolv40
---------------------------------------------------------------------
 # b3lyp empiricaldispersion=gd3bj def2tzvp geom=allcheck guess=read TD
 =(Nstates=40) scrf=(pcm,solvent=THF)
 ---------------------------------------------------------------------

Excitation energies and oscillator strengths:
 Excited State  1:      Singlet-A     1.9015 eV  652.05 nm  f=0.0080  <S**2>=0.000
     191 -> 193        0.39300
     192 -> 193        0.57818
 This state for optimization and/or second-order correction.
 Total Energy, E(TD-HF/TD-DFT) =  -5100.00652260
 Copying the excited state density for this state as the 1-particle RhoCI density.
```

```
Excited State  2:      Singlet-A     2.4378 eV  508.59 nm  f=0.0252  <S**2>=0.000
   191 -> 193       0.49960
   192 -> 193      -0.30905
   192 -> 194       0.22975
   192 -> 197      -0.19047

Excited State  3:      Singlet-A     2.6358 eV  470.38 nm  f=0.0019  <S**2>=0.000
   191 -> 195      -0.14340
   192 -> 194      -0.23205
   192 -> 195       0.63631

Excited State  4:      Singlet-A     2.7355 eV  453.24 nm  f=0.0284  <S**2>=0.000
   191 -> 193      -0.19366
   191 -> 194      -0.21299
   191 -> 197       0.16918
   192 -> 193       0.14501
   192 -> 194       0.44258
   192 -> 195       0.18222
   192 -> 196      -0.11701
   192 -> 197      -0.29303

Excited State  5:      Singlet-A     2.9545 eV  419.64 nm  f=0.0066  <S**2>=0.000
   191 -> 195       0.32869
   191 -> 200      -0.17762
   192 -> 200       0.55118
   192 -> 201       0.15498

Excited State  6:      Singlet-A     2.9767 eV  416.51 nm  f=0.0107  <S**2>=0.000
   192 -> 194       0.32959
   192 -> 197       0.44971
   192 -> 198       0.16042
   192 -> 199       0.32167
   192 -> 201       0.10298

Excited State  7:      Singlet-A     3.1074 eV  398.99 nm  f=0.0028  <S**2>=0.000
   191 -> 194       0.20456
   191 -> 195       0.49765
   191 -> 197      -0.21154
   191 -> 200       0.19063
   191 -> 201       0.12633
   192 -> 195       0.11808
   192 -> 200      -0.25719

Excited State  8:      Singlet-A     3.2029 eV  387.10 nm  f=0.0090  <S**2>=0.000
   191 -> 194       0.16094
   192 -> 194       0.19913
   192 -> 196       0.61028
   192 -> 199      -0.13958

Excited State  9:      Singlet-A     3.2927 eV  376.55 nm  f=0.0775  <S**2>=0.000
   191 -> 194       0.29297
   191 -> 195      -0.18912
   191 -> 197      -0.17149
   191 -> 199      -0.11290
   192 -> 194       0.18856
   192 -> 196      -0.28685
   192 -> 197       0.16987
   192 -> 198      -0.23253
   192 -> 199      -0.21100
   192 -> 200       0.15037
   192 -> 201      -0.12127
   192 -> 203      -0.13319

Excited State 10:      Singlet-A     3.3750 eV  367.36 nm  f=0.0227  <S**2>=0.000
   191 -> 194      -0.15055
   191 -> 195       0.13496
   191 -> 197       0.28406
   191 -> 198       0.10153
   191 -> 199       0.22818
   191 -> 203       0.10562
```

```
   192 -> 193      -0.10111
   192 -> 197       0.34556
   192 -> 198      -0.22459
   192 -> 199      -0.26449

Excited State  11:      Singlet-A      3.4425 eV  360.16 nm  f=0.0012  <S**2>=0.000
   191 -> 197       0.11080
   191 -> 199       0.12640
   191 -> 200       0.58155
   191 -> 201       0.18659
   192 -> 200       0.23980

Excited State  12:      Singlet-A      3.4778 eV  356.50 nm  f=0.0790  <S**2>=0.000
   191 -> 194       0.40401
   191 -> 197       0.32403
   191 -> 199       0.16158
   192 -> 196      -0.11148
   192 -> 198       0.38380

Excited State  13:      Singlet-A      3.5166 eV  352.57 nm  f=0.0563  <S**2>=0.000
   191 -> 194      -0.26951
   191 -> 197      -0.18335
   192 -> 198       0.46089
   192 -> 199      -0.36531

Excited State  14:      Singlet-A      3.6321 eV  341.36 nm  f=0.0245  <S**2>=0.000
   191 -> 194       0.10535
   191 -> 196       0.53926
   191 -> 199      -0.11860
   192 -> 199      -0.21807
   192 -> 201       0.31188

Excited State  15:      Singlet-A      3.6785 eV  337.05 nm  f=0.0138  <S**2>=0.000
   191 -> 196      -0.41403
   191 -> 197       0.15713
   191 -> 198      -0.11052
   191 -> 199      -0.11044
   192 -> 199      -0.20039
   192 -> 201       0.42427

Excited State  16:      Singlet-A      3.7710 eV  328.78 nm  f=0.0012  <S**2>=0.000
   192 -> 201       0.19205
   192 -> 202       0.64626
   192 -> 203      -0.14998

Excited State  17:      Singlet-A      3.8423 eV  322.68 nm  f=0.0416  <S**2>=0.000
   189 -> 193       0.13986
   191 -> 197      -0.23927
   191 -> 198       0.45516
   191 -> 199       0.18297
   192 -> 201       0.21968
   192 -> 202      -0.20683
   192 -> 203      -0.19227

Excited State  18:      Singlet-A      3.9145 eV  316.73 nm  f=0.0015  <S**2>=0.000
   189 -> 193      -0.14141
   191 -> 198       0.47422
   191 -> 199      -0.25352
   192 -> 201      -0.13235
   192 -> 202       0.10060
   192 -> 203       0.34467

Excited State  19:      Singlet-A      3.9264 eV  315.77 nm  f=0.0270  <S**2>=0.000
   189 -> 193       0.48095
   190 -> 193      -0.18031
   191 -> 199       0.17382
   192 -> 199      -0.10153
   192 -> 201      -0.10333
   192 -> 202       0.10304
   192 -> 203       0.33920
```

Excited State 20: Singlet-A 4.0184 eV 308.54 nm f=0.0739 <S**2>=0.000

189 -> 193	-0.28460
190 -> 193	0.19534
191 -> 197	-0.19868
191 -> 199	0.44391
191 -> 201	-0.10812
191 -> 203	-0.11551
192 -> 203	0.23449

Table S18. Representation of the most important molecular orbitals of **5**.

LUMO+7 (167) 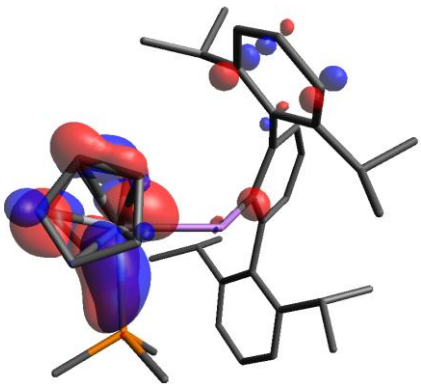	LUMO+6 (166) 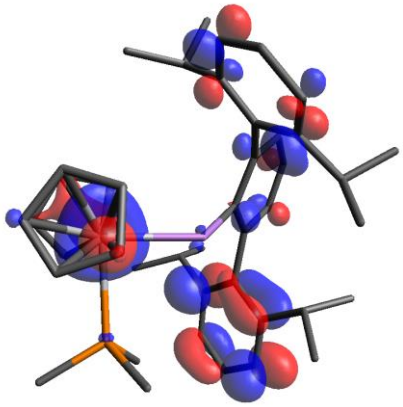
LUMO+5 (165) 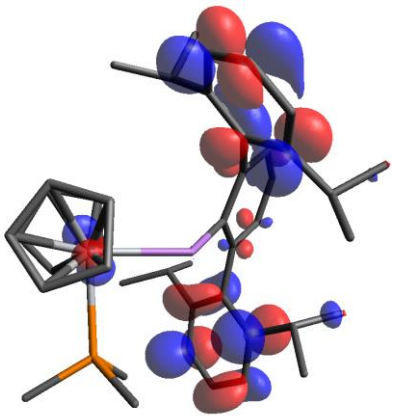	LUMO+4 (164) 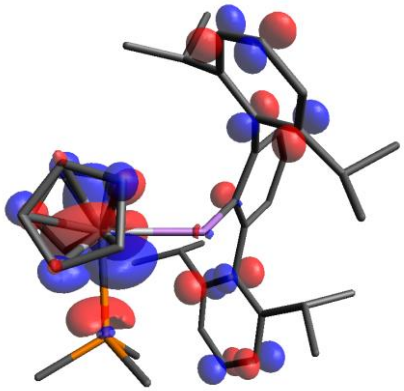
LUMO+3 (163) 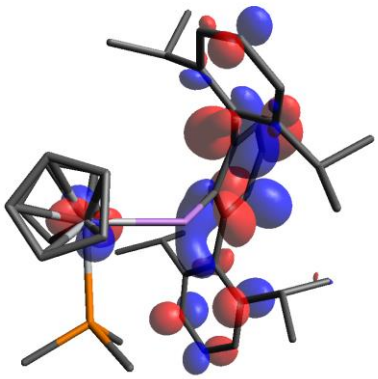	LUMO+2 (162) 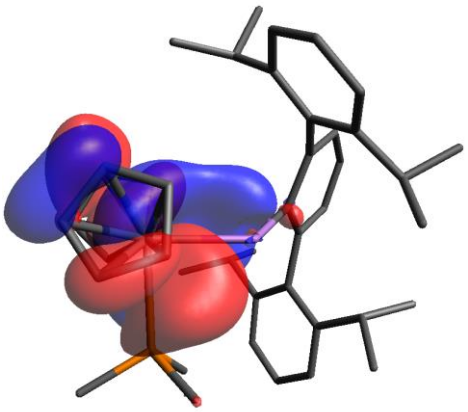
LUMO+1 (161)	LUMO (160)

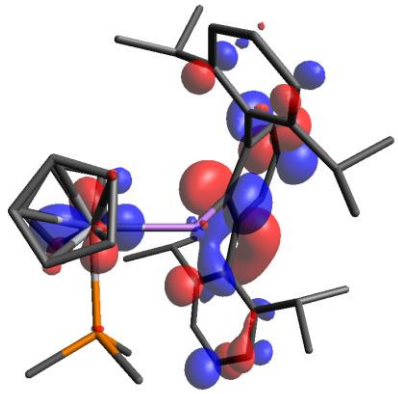	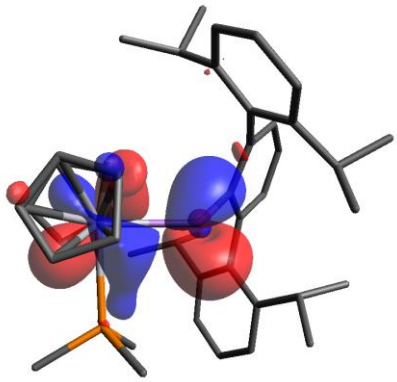
HOMO (159)	HOMO-1 (158)
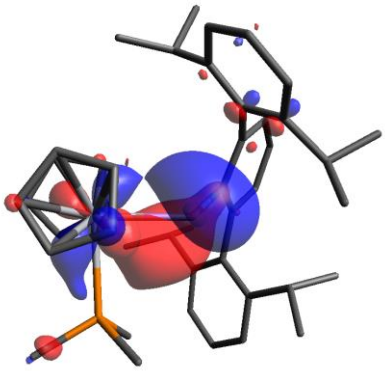	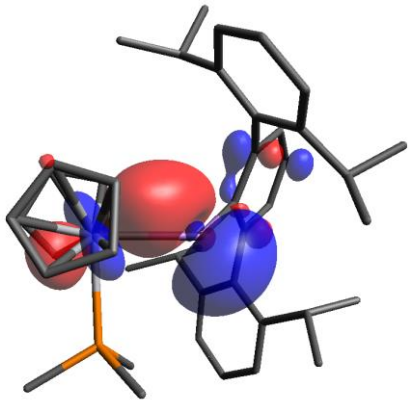

6 References

1 M. Fischer, L. Vincent-Heldt, M. Hillje, M. Schmidtmann and R. Beckhaus, Dalton Trans. **2020**, *49*, 2068-2072

2 P. Gupta, J.-E. Siewert, T. Wellnitz, M. Fischer, W. Baumann, T. Beweries and C. Hering-Junghans, *Dalton Trans.* **2021**, *50*, 1838-1844.

3 M. Fischer, S. Nees, T. Kupfer, J. T. Goettel, H. Braunschweig and C. Hering.Junghans *J. Am. Chem. Soc.* **2021**, http://dx.doi.org/10.1021/jacs.1c00204.

4 G. M. Sheldrick, *Acta Cryst. A* **2015**, *71*, 3–8.

5 G. M. Sheldrick, *Acta Cryst. C* **2015**, *71*, 3–8.

6 G. M. Sheldrick, *SADABS Version 2*, University of Göttingen, Germany, **2004**.

7 A. L. Spek, *Acta Cryst.* **2015**, *C71*, 9–18

8 *Gaussian 16, Revision C.01,* M. J. Frisch, G. W. Trucks, H. B. Schlegel, G. E. Scuseria, M. A. Robb, J. R. Cheeseman, G. Scalmani, V. Barone, G. A. Petersson, H. Nakatsuji, X. Li, M. Caricato, A. V. Marenich, J. Bloino, B. G. Janesko, R. Gomperts, B. Mennucci, H. P. Hratchian, J. V. Ortiz, A. F. Izmaylov, J. L. Sonnenberg, D. Williams-Young, F. Ding, F. Lipparini, F. Egidi, J. Goings, B. Peng, A. Petrone, T. Henderson, D. Ranasinghe, V. G. Zakrzewski, J. Gao, N. Rega, G. Zheng, W. Liang, M. Hada, M. Ehara, K. Toyota, R. Fukuda, J. Hasegawa, M. Ishida, T. Nakajima, Y. Honda, O. Kitao, H. Nakai, T. Vreven, K. Throssell, J. A. Montgomery, Jr., J. E. Peralta, F. Ogliaro, M. J. Bearpark, J. J. Heyd, E. N. Brothers, K. N. Kudin, V. N. Staroverov, T. A. Keith, R. Kobayashi, J. Normand, K. Raghavachari, A. P. Rendell, J. C. Burant, S. S. Iyengar, J. Tomasi, M. Cossi, J. M. Millam, M. Klene, C. Adamo, R. Cammi, J. W. Ochterski, R. L. Martin, K. Morokuma, O. Farkas, J. B. Foresman, and D. J. Fox, Gaussian, Inc., Wallingford CT, **2016**.

9 a) E. D. Glendening, J. K. Badenhoop, A. E. Reed, J. E. Carpenter, J. A. Bohmann, C. M. Morales, C. R. Landis and F. Weinhold, *NBO 6.0*, Theoretical Chemistry Institute, University of Wisconsin, Madison, **2013**; b) J. E. Carpenter and F. Weinhold, *J. Mol. Struct.: THEOCHEM* **1988**, *169*, 41–62; c) F. Weinhold and J. E. Carpenter, *The Structure of Small Molecules and Ions*, Plenum Press, **1988**; d) F.

Weinhold and C. R. Landis, *Valency and Bonding. A Natural Bond Orbital Donor-Acceptor Perspective*, Cambridge University Press, **2005**.

10 a) A. D. Becke, *Phys. Rev. A* **1988**, *38*, 3098–3100; b) J. P. Perdew, *Phys. Rev. B* **1986**, *33*, 8822–8824.

11 a) S. H. Vosko, L. Wilk and M. Nusair, *Can. J. Phys.* **1980**, *58*, 1200–1211; b) C. Lee, W. Yang and R. G. Parr, *Phys. Rev. B* **1988**, *37*, 785–789; c) B. Miehlich, A. Savin, H. Stoll and H. Preuss, *Chem. Phys. Lett.* **1989**, *157*, 200–206; d) A. D. Becke, *J. Chem. Phys.* **1993**, *98*, 5648–5652.

12 F. Weigend and R. Ahlrichs, *Phys. Chem. Chem. Phys.* **2005**, *7*, 3297–3305.

13 a) S. Grimme, J. Antony, S. Ehrlich and H. Krieg, *J. Chem. Phys.* **2010**, *132*, 154104; b) S. Grimme, S. Ehrlich and L. Goerigk, *J. Comput. Chem.* **2011**, *32*, 1456–1465.

14 T. Lu and F. Chen, *J. Comput. Chem.* **2012**, *33*, 580.

15 GaussView, Version 6.1, Roy Dennington, Todd A. Keith, and John M. Millam, Semichem Inc., Shawnee Mission, KS, **2016**

16 a) R. F. W. Bader, *Acc. Chem. Res.* **1985**, *18*, 9–15; b) R. F. W. Bader, *Chem. Rev.* **1991**, *91*, 893–928; c) R. F. W. Bader, *Atoms in Molecules: A Quantum Theory*, Oxford University Press, **1994**; d) R. F. W. Bader, *Monatsh. Chem.* **2005**, *136*, 819–854.

17 a) C. J. Cramer, *Essentials of Computational Chemistry: Theories and Models*, John Wiley & Sons, Ltd, Chichester, UK, **2004**; b) L. Salem and C. Rowland, C. *Angew. Chem. Int. Ed. Engl.* **1972**, *11*, 92–111; c) J.-P. Malrieu and G. Trinquier, *J. Phys. Chem. A* **2012**, *116*, 8226–8237.

18 E. Miliordos, K. Ruedenberg and S. S. Xantheas, S. S. *Angew. Chem. Int. Ed.* **2013**, *52*, 5736–5739.

19 a) L. Noodleman, *J. Chem. Phys.* **1981**, *74*, 5737–5743; b) D. Herebian, K. E. Wieghardt and F. Neese, *J. Am. Chem. Soc.* **2003**, *125*, 10997–11005; c) M. Abe, *Chem. Rev.* **2013**, *113*, 7011–7088.

20 G. Zhao, F. Basuli, U. J. Kilgore, H. Fan, H. Aneetha, J. C. Huffman, G. Wu and D. J. Mindiola, *J. Am. Chem. Soc.* **2006**, *128*, 13575-13585.

21 a) F. London, *J. Phys. Radium* **1937**, *8*, 397–409; b) R. McWeeny, *Phys. Rev.* **1962**, *126*, 1028–1034; c) R. Ditchfield, *Mol. Phys.* **1974**, *27*, 789–807; d) K. Wolinski, J. F. Hinton and P. Pulay, *J. Am. Chem. Soc.* **1990**, *112*, 8251–8260; e) J. R.

Cheeseman, G. W. Trucks, T. A. Keith and M. J. Frisch, *J. Chem. Phys.* **1996**, *104*, 5497–5509.

22 C. J. Jameson, A. De Dios and A. Keith Jameson, *Chem. Phys. Lett.* **1990**, *167*, 575–582.

23 C. van Wüllen, *Phys. Chem. Chem. Phys.* **2000**, *2*, 2137–2144.